Journal of Physics D: Applied Physics

TOPICAL REVIEW

Recent advances in the growth of gallium oxide thin films employing various growth techniques—a review

To cite this article: B R Tak *et al* 2021 *J. Phys. D: Appl. Phys.* **54** 453002

IOP Publishing Journal of Physics D: Applied Physics
J. Phys. D: Appl. Phys. **54** (2021) 453002 (22pp) https://doi.org/10.1088/1361-6463/ac1af2

Topical Review

Recent advances in the growth of gallium oxide thin films employing various growth techniques—a review

B R Tak[1], Sudheer Kumar[1], A K Kapoor[1], Danhao Wang[2], Xiaohang Li[3], Haiding Sun[2] and R Singh[1,*]

[1] Department of Physics, Indian Institute of Technology Delhi, Hauz Khas, New Delhi 110016, India
[2] School of Microelectronics, University of Science and Technology of China, Hefei, Anhui 230026, People's Republic of China
[3] Advanced Semiconductor Laboratory, King Abdullah University of Science and Technology (KAUST), Thuwal 23955-6900, Saudi Arabia

E-mail: rsingh@physics.iitd.ac.in

Received 11 March 2021, revised 2 July 2021
Accepted for publication 5 August 2021
Published 23 August 2021

Abstract

Gallium oxide (Ga_2O_3) is rapidly emerging as a material of choice for the development of solar blind photodetectors and power electronic devices which are particularly suitable in harsh environment applications, owing to its wide bandgap and extremely high Baliga figure of merit. The Ga_2O_3 based devices show robustness against chemical, thermal and radiation environments. Unfortunately, the current Ga_2O_3 technology is still not mature for commercial usage. Thus, extensive research on the growth of various polymorph of Ga_2O_3 materials has been carried out. This article aims to provide an overview of the current understanding of epitaxial growth of different phases of Ga_2O_3 by various growth techniques including pulsed laser deposition, molecular beam epitaxy, metal-organic chemical vapor deposition, sputtering, mist chemical vapor deposition and atomic layer deposition. The review also investigates the factors such as the growth temperature, pressure, carrier gas, III/V ratio, substrate as well as doping which would influence the synthesis and the stability of meta stable phases of Ga_2O_3. In addition, a thorough discussion of growth window is also provided using phase diagrams for aforementioned epitaxial deposition methods.

Keywords: gallium oxide, MOCVD, MBE, PLD, sputtering, mist CVD, ALD

(Some figures may appear in color only in the online journal)

1. Introduction

Similar to gallium nitride (GaN) and silicon carbide (SiC) semiconductors [1–4], gallium oxide (Ga_2O_3) is being pursued as a viable alternative material for several applications due to its large bandgap, extremely high Baliga figure of merit (BFOM) and relatively inert nature. Moreover, the Ga_2O_3 possesses six polymorphs α, β, γ, δ, ε, and κ depending on the growth conditions [5–11]. In the past 15 years, various devices have been fabricated and demonstrated using Ga_2O_3 material that include field effect transistors (FETs) [12–15], metal-oxide-semiconductor field effect transistors (MOSFETs) [16–19], photodetectors [20–31] and Schottky barrier diodes [32–37]. These devices are mainly useful for defense and space applications such as radar,

* Author to whom any correspondence should be addressed.

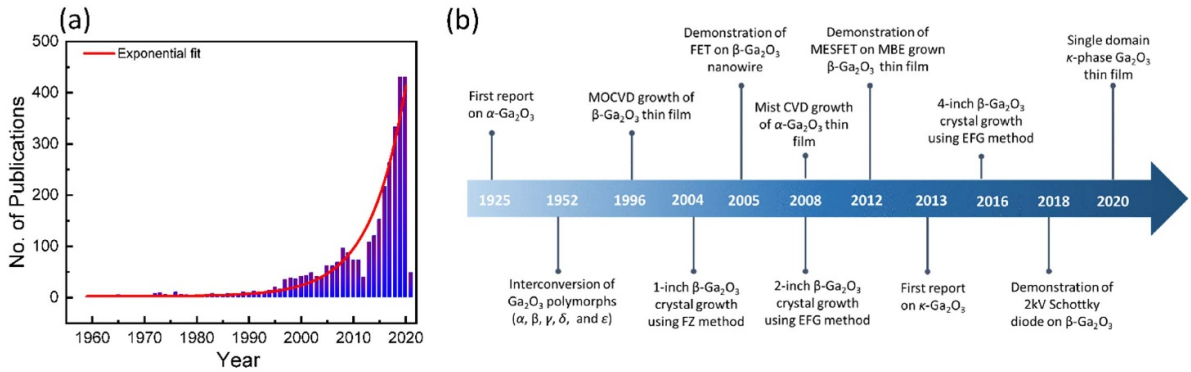

Figure 1. (a) Statistical graph of research outcome of Ga_2O_3 material as a function of number of publications per year. Data extracted from Scopus with keywords gallium oxide and Ga_2O_3. (b) The timeline of breakthrough milestones achieved in Ga_2O_3 material research and technology.

jamming, countermeasure, missile detection and wireless communication [38, 39]. Therefore, research on Ga_2O_3 materials and devices has been increasing exponentially with time, as evident from figure 1(a) (statistical data was extracted from Scopus), exhibiting the growing number of publications related with Ga_2O_3 material and its corresponding implementation for various devices as-mentioned above. The timeline of major milestones achieved in Ga_2O_3 material research and development is displayed in figure 1(b) [9, 14, 40–51]. In the last century, research has been progressed from growth and stabilization of different phases of Ga_2O_3 to its realization of state of the arts high power devices. Large area growth of single crystal substrates was the most important breakthrough achievement for advancement of current Ga_2O_3 technology.

In fact, the Ga_2O_3 technology has a huge advantage over GaN due to the availability of large size free standing single crystals. The Novel Crystal Technologies in Japan has demonstrated six-inch β-Ga_2O_3 (001) single crystal substrates using melt growth methods [48, 52]. However, single crystal substrates of other phases have not been obtained using melt growth till date and most of them are synthesized via heteroepitaxial growth. During the last 2 decades, many growth techniques or methods have been employed to synthesize bulk β-Ga_2O_3 single crystal [47, 48], thin films [53–59], and nanostructures [60–62]. For bulk single crystal fabrication, well established melt growth techniques such as Czochralski (CZ), floating-zone (FZ), and edge-defined film fed growth (EFG) have been utilized and well established [43, 45, 63–67]. For the growth of nanostructures various techniques have been developed, such as physical evaporation in which evaporation of bulk gallium metal target under controlled conditions occurs; laser ablation growth which occurs without foreign catalyst [68], arc-discharge by the electrical discharge of GaN powders mixed with small amount of transition metals [69, 70], thermal chemical vapor deposition (CVD) by evaporating pure gallium metal as Ga vapor source under different conditions in a tubular furnace [71, 72], carbothermal reduction [73], metal organic CVD using a single source organometallic precursor at low temperature [74], and microwave plasma [75] method. This article covers the review of basic properties of Ga_2O_3 polymorphs such as crystal structures, electronic band structure, and electrical and optical properties. More importantly, various growth techniques of thin films and epitaxial layers, including metal-organic chemical vapor deposition (MOCVD), molecular beam epitaxy (MBE), pulsed laser deposition (PLD), sputtering, mist chemical vapor deposition (mist CVD) and atomic layer deposition (ALD) will be discussed in detail. Finally, the future research opportunities and the outlook of Ga_2O_3 related technology will be described.

2. Material properties of Ga_2O_3

In this section, a brief introduction of the basic properties of Ga_2O_3 polymorphs such as crystal structure, electric and optical properties are described. The physical properties of all Ga_2O_3 polymorphs are shown in table 1.

2.1. Phase conversion and phase stability

Among all the six phases, only β-phase is the most stable thermodynamically. All the other polymorphs are metastable and get converted into β-phase upon thermal treatment from 300 °C to 870 °C [76]. The formation energies of all the phases follow $\beta > \varepsilon > \alpha > \delta > \gamma$ order [10]. Roy *et al* reported the interconversion of five polymorphs (α, β, γ, δ and ε) of Ga2O3 using Gallia and its hydrates [41]. The flow chart of these phases is shown in figure 2. After almost 60 years, Playford *et al* have synthesized Ga_2O_3 polymorphs using solvothermal process of gallium metal and performed structural investigation on these phases. In this study, they have found new phase named as κ-Ga_2O_3 by thermal treatment of $Ga_5O_7(OH)$ at 500 °C.

In the beginning, single crystals of α-phase were obtained by applying 4.4 GPa pressure at 1000 °C on β-Ga_2O_3 powder [77]. The stable α-phase was achieved by quenching it at room temperature and atmospheric pressure. Again, heating these crystals above 600 °C resulted in transformation to β-phase. Lee *et al* also reported α–β phase conversion above 600 °C [78]. Ma *et al* reported the conversion of β–α phase under cold compression with higher pressure of 19.2 GPa [79]. Recently,

Table 1. Material properties of Ga_2O_3 polymorphs.

	α	β	γ	δ	ε	κ
Crystal structure	Corundum	Monoclinic	Cubic defective spinel	Cubic subgroup of ε	Pseudo hexagonal	Orthorhombic, subgroup of ε
Lattice parameters (Å)	$a = b = 4.98$–5.04, $c = 13.43$–13.62	$a = 12.12$–12.34, $b =$ 3.03 and 3.04, $c = 5.80$–5.87	$a = 8.24$–8.30	$a = 9.4$–10	$a = 2.90$, $c = 9.25$	$a = 5.05$, $b = 8.69$, $c = 9.27$
Space group	$R\bar{3}m$	C2/m	$Fd\bar{3}m$	Ia3	P63mc	$Pna2_1$
Bandgap (eV)	5.2 and 5.3	4.5–4.9	4.5–5.0	—	4.5–5.0	4.6–4.9
Refractive index (n)	1.74–1.95	1.68–1.89	2.0 and 2.1	1.8	1.6	—
Density (g cm^{-3})	6.48	5.94	5.76–5.93	4.98–5.18	5.88–6.06	—
Effective mass (m_e^*)	$0.276m_0$	$0.342m_0$	—	—	$0.24m_0$	—
Electron mobility (cm^2 V s^{-1})	24	200	1.6	—	—	—
Thermal conductivity (W cm^{-1} K)	—	0.27 (010), 0.11 (100)	—	—	—	—
Bulk modulus	185	150	—	160	160	—
Polarization (μC cm^{-2})	—	—	—	—	24	26
Doping (cm^{-3})	10^{17}–10^{20}	10^{17}–10^{20}	1.8×10^{19}	—	10^{17} and 10^{18}	—

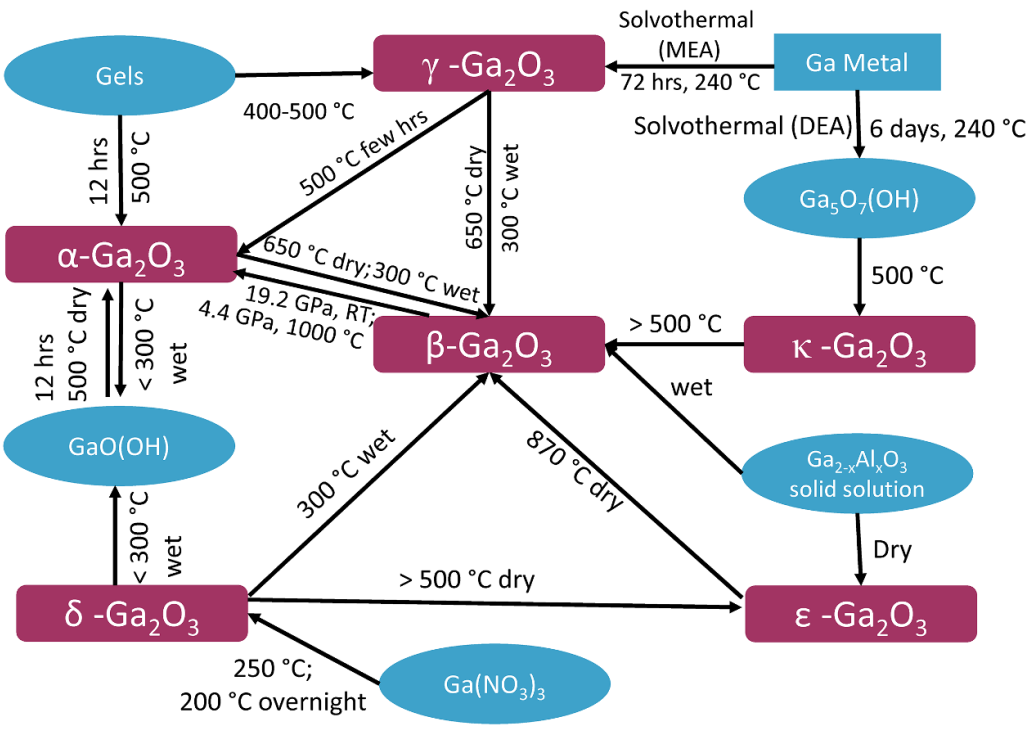

Figure 2. Interconversion of Ga_2O_3 polymorphs and its hydrates. Conversion of $Ga_{2-x}Al_xO_3$ occurs only where $x < 1.3$; where $x > 1.3$, α-Al_2O_3 formation occurs. Reprinted with permission from [41]. Copyright (1952) American Chemical Society. [9] John Wiley & Sons. Copyright © 2013 WILEY-VCH Verlag GmbH & Co. KGaA, Weinheim.

Jinno *et al* reported thermal stability of α-$(Al_xGa_{1-x})_2O_3$ thin films. The phase transition from α to β was not found up to 1100 °C for $x > 0.65$. Hence, higher Al composition thermally stabilizes into the α-phase [80]. For stabilization of γ-phase, Liu *et al* reported Cu doping of 12.5 at% in Ga_2O_3 which resulted in stable crystalline γ-phase at 700 °C. Further increase in temperature to 800 °C tend to conversion in stable β-Ga_2O_3 [81]. Hayashi *et al* have also found stable γ-Ga_2O_3 thin films in 7% Mn doped samples whereas undoped films showed β-phase structure. Stable epitaxial growth of undoped γ-Ga_2O_3 thin films were carried out only on $MgAl_2O_4$ (100) substrate using mist CVD [82].

2.2. Crystal structures and their physical properties

The crystal structure of β-Ga_2O_3 was investigated by Geller in 1960 [83]. He found that it has base-centered monoclinic crystal structure with cell dimensions $a = 12.12$–12.34, $b = 3.03$ and 3.04 Å, $c = 5.80$–5.87 Å and $\beta = 103.7° \pm 0.3°$. Its unit cell has the space group symmetry of C2/m.

In the unit cell of β-Gallia structure, two crystallographically non-equivalent Ga atoms are positioned at tetrahedral and octahedral sites [84]. The oxygen ions are situated in a distorted cubic closed pack array. Three crystallographically non-equivalent oxygen atoms are situated at trigonal [O(I) and O(II)] and tetrahedral [O(III)] sites. This leads to anisotropy in physical, optical, and electrical properties along different directions. For example, it has been reported that thermal conductivity along (010) direction is higher than that in (100) direction [85–87]. Also, the bandgap shows pronounced anisotropy, though not much has been reported on its values along the *a, b,* and *c* crystallographic directions. Ricci *et al* have shown a bandgap anisotropy by measuring the absorption with polarization parallel to three crystallographic axes [88]. They showed that lowest bandgap is 4.54 eV in the direction $E \| c$, followed by 4.57 eV in $E \| a$, and $E \| b$ was at 4.72 eV. This showed a clear anisotropy in the bandgap of β-Ga_2O_3. Alongside the anisotropy, bulk β-Ga_2O_3 suffers from cleavage which is another drawback of β-phase. Moreover, homoepitaxy in (100) orientation is susceptible to high density of twin boundaries which limits the electrical properties like conductivity and mobility.

Epitaxial growth of α-Ga_2O_3 on sapphire has the possibility of providing better crystalline quality due to similar crystal structure of sapphire as well as lower lattice mismatch than the other phases. The α-Ga_2O_3 is a corundum (hexagonal) phase in which all gallium ions are iso-structurally coordinated on octahedral sites [10]. The symmetric structure of α-phase drives more homogeneous electrical, optical and physical properties than β-phase. The space group of α-phase investigated by He *et al* is $R\bar{3}m$ [89]. The lattice constants of α-Ga_2O_3 are $a = b = 4.98$–5.04 and $c = 13.43$–13.62 Å. Unit cell of α-phase is denser than β-phase due to shorter distance between Ga atoms. The density of α and β phases are 6.48 and 5.94 gm cm^{-3}, respectively. Relatively lower electron effective mass of α-Ga_2O_3 ($0.276m_0$) is reported than β-Ga_2O_3 ($0.342m_0$) [89]. The bandgap of unintentionally doped (UID) α-Ga_2O_3 has been reported to be 5.2 and 5.3 eV.

The crystal structure of γ-Ga_2O_3 was initially explored by Playford *et al* [7]. The unit cell has cubic spinel structure with $Fd\bar{3}m$ crystal symmetry. Gallium atom in the unit cell occupies octahedral and tetrahedral positions (ideal spinel and non-spinel). Oshima *et al* have investigated the optical properties of defective spinel γ-phase [82]. They reported refractive index of 2.0 and 2.1 and direct and indirect bandgap of 5.0 and 4.4 eV, respectively. In 2015, authors were successful to demonstrate n-type conductivity in γ-Ga_2O_3 using silicon doping [90]. The thin films grown on spinel $MgAl_2O_4$ showed carrier concentration of 1.8×10^{19} cm^{-3} with Hall mobility of 1.6 cm^2 V^{-1} s^{-1} at room temperature. Hayashi *et al* reported that the 7% Mn doped γ-Ga_2O_3 films showed ferromagnetism from room temperature to 350 K [91].

Additionally, the research progress on δ-phase of Ga_2O_3 is not so advanced due to difficulty in phase stabilization. The thin film growth of δ-phase has not been realized till date. Roy *et al* suggested bixbyite crystal structure similar to C-type rare earths with space group of Ia3 [41]. They observed lattice constant $a = 10$ Å for this phase. However, Yoshioka *et al* predicted $a = 9.4$ Å using density functional theory (DFT) [10]. In the later years, Playford *et al* have concluded using neutron diffraction that δ-phase is only the nanocrystalline form of ε-Ga_2O_3 [9]. The density of δ-Ga_2O_3 was reported to be 4.98 and 5.18 gm cm^{-3} as calculated from x-ray data and pycnometer, respectively [41].

The real structure of ε-Ga_2O_3 was investigated by Cora *et al* using high resolution TEM and x-ray diffraction (XRD) [8]. The authors concluded that ε-Ga_2O_3 has orthorhombic crystal structure of P63mc space group. The lattice constants of ε-phase are $a = 5.12$, $b = 8.79$ and $c = 9.41$. The optical bandgap of 4.9–5.0 eV is reported for ε-phase and can be engineered from 4.5 to 5.9 eV using In and Al doping [92–95]. The ε-phase is one of the most interesting phases of Ga_2O_3 due to its piezoelectric, pyroelectric and ferroelectric nature. A large spontaneous polarization of 24.4 μC cm^{-2} was theoretically predicted which is as good as $BaTiO_3$ [96]. Mezzadri *et al* first time measured the ferroelectricity in ε-phase which makes this material a unique combination of ferroelectricity and semiconducting properties [11]. A large dielectric constant of 32 was reported for ε-Ga_2O_3 which is almost three times higher than β-Ga_2O_3 [94]. The first principle calculations were employed to estimate electron effective mass of ε-phase. Authors reported an isotropic effective mass of $0.24m_0$ [97]. Mulazzi *et al* have calculated the hole effective mass of $4.2m_0$ at γ-point using photoelectron spectroscopy [98].

For the study of other phases, Playford *et al* published first report on κ-phase Ga_2O_3 in 2013 [9]. Authors found κ-Ga_2O_3 with the mixture of β-phase and could not succeeded to get pure phase. The lattice parameters of unit cell were calculated using Le Bail profile refinement. The unit cell possesses orthorhombic crystal structure having lattice parameters $a = 5.05$, $b = 8.69$ and $c = 9.27$ Å. It has space group of $Pna2_1$. Later, Cora *et al* investigated the crystal structure using HRTEM and confirmed that κ-phase exists as a nanocrystalline (5–10 nm domains) form in the ε-phase [8]. The oxygen atoms were positioned as ABAC type closed packed stacking and Ga atoms situated at tetrahedral and octahedral sites. The Ga atoms forms one layer of pure octahedral site and another layer mixed with both octa and tetrahedral sites. Kim *et al* have reported the bandgap of 4.62 eV and spontaneous polarization of 26.39 μC cm^{-2} using DFT [96].

3. Growth techniques for Ga_2O_3 thin films

Advances in large area bulk crystal growth of required diameter and low defect density are the mainly driving aggressive research for application of this material for power electronics

Table 2. Epitaxial and melt growth methods for all phases of Ga_2O_3.

Phases	Epitaxial growth methods	Melt grown bulk substrates	References
α	Mist CVD, MOCVD, HVPE, ALD	No	[58, 100–108]
β	MBE, MOCVD, PLD, HVPE, sputtering, ALD	Up to six inch (EFG, CZ, FZ)	[13, 52, 54, 55, 108–119]
γ	PLD, mist CVD	No	[90, 120–122]
δ	Chemical reactions	No	[9]
ε	Mist CVD, MOCVD, HVPE, sputtering	No	[59, 123–128]
κ	PLD, mist CVD, HVPE, MOCVD, ALD	No	[108, 129–134]

and solar blind detection. High-quality crystals with required insulating or semiconducting properties can be grown by EFG, CZ, or by FZ growth methods. Each method is capable of producing large area high-quality crystals with a demonstration of 2″–6″ crystal size [13, 52]. Single crystal substrates of only β-Ga_2O_3 are available using melt growth method as displayed in table 2. The low cost of synthesizing Ga_2O_3 material is another major criterion for its increased interest in power electronics in comparison to the SiC and GaN. The grown crystals can be cut in technologically important orientations like ($\bar{2}01$), (010), and (100) which are mostly used in device applications. In addition, there is also considerable progress in the epilayer growth using a number of techniques like MOCVD, HVPE, PLD, mist CVD and MBE. Table 2 summarizes the epitaxial and melt growth methods to grow all six phases of Ga_2O_3. In this section, we will discuss various deposition techniques of Ga_2O_3 thin films. The melt-growth methods can be found in other reports [48, 99].

3.1. PLD

In this process, laser pulses are used to ablate the material from a target. Cylindrical sintered pellets are used as a target. As the laser beam is incident on target, a plasma plume is created which is directed normally towards the substrate. Substrate is situated in front of target at a distance of a few 10 mm. It is very easy to tailor the content in deposited films by changing its amount in target material. PLD is a promising technique for the deposition of high-quality films at low growth temperatures of 200 °C–800 °C. The crystalline quality of PLD grown thin films depends on various parameters such as laser energy, growth temperature and growth pressure. Therefore, an optimum combination of all these parameters is essential to grow high quality thin films. Generally, PLD does not require an ultrahigh vacuum (UHV) atmosphere. Typically, KrF excimer ($\lambda = 248$ nm) and Nd:YAG ($\lambda = 266$ nm) lasers are used for the ablation of Ga_2O_3 targets. In the past, only β-phase of gallium oxide was possible to be grown using PLD. However, Grundman *et al* has been successful to grow orthorhombic κ-phase using tin-assisted PLD method [130, 135, 136]. Authors proposed surfactant mediated epitaxy growth mechanism for κ-Ga_2O_3 growth.

Moreover, the Ga_2O_3 thin films have been deposited on various rigid as well as flexible substrates using PLD. In case of heteroepitaxy on *c*-plane sapphire, the lowest reported FWHM of rocking curve for ($\bar{2}01$) plane is 359 arcsec [137]. This film was grown at 800 °C substrate temperature using 2.4 J cm^{-2} laser energy. Similarly, the lowest achieved FWHM of rocking curve for homoepitaxial β-Ga_2O_3 (010) is 21 arcsec [138]. This homoepitaxial growth was performed with 3 J cm^{-2} laser energy at 550 °C substrate temperature. On flexible substrates, a few PLD growths of Ga_2O_3 have also been reported. Amorphous Ga_2O_3 thin film growth on muscovite was recently reported by Tak *et al* [139]. In their further work, authors have also demonstrated the epitaxial growth of β-Ga_2O_3 thin films on muscovite substrate which is the first time epitaxial growth on any flexible substrate [53]. Both the growths were performed at 600 °C substrate temperature. In comparison to amorphous film, authors increased the laser energy from 1.2 J cm^{-2} to 1.5 J cm^{-2} and decreased the laser frequency from 10 Hz to 5 Hz to fabricate epitaxial β-Ga_2O_3. Figure 3(a) shows ($\bar{2}01$) orientation of β-Ga_2O_3 thin films fabricated on muscovite mica. The rocking curve measurement of ($\bar{2}01$) plane was also recorded. The FWHM of 1.3° was reported for flexible β-Ga_2O_3 thin films.

Previously, Yu *et al* [137] and Ou *et al* [140] deposited epitaxial β-Ga_2O_3 thin films on *c*-sapphire (0001) under oxygen partial pressure of 200 mT and 50 mT, respectively. Both the groups have used KrF excimer laser ($\lambda = 248$ nm and frequency = 10 Hz) with pulse energy density 2.4 J cm^{-2} as a laser source. The epitaxial nature of pulsed laser deposited β-Ga_2O_3 thin films substantially depends on substrate temperature and pressure conditions. They concluded that films grown up to 400 °C substrate temperature were amorphous. As substrate temperature increased from 400 °C to 850 °C, the ad-atoms get enough thermal energy for surface migration which leads to growth of ($\bar{2}01$) oriented films. Further increasing temperature to 1000 °C, the atomic arrangement gets destroyed. The XRD pattern shows some extra peaks of (400) and ($\bar{8}01$) planes which are the indication of polycrystalline phase of β-Ga_2O_3. In [140], Ou *et al* found the highest crystalline quality film at substrate temperature of 850 °C as shown in figure 3(c). An abrupt absorption edge at a deep UV region (around 250 nm) was also observed for the films grown at temperature 550 °C–1000 °C as shown in figure 3(d).

Recently, Tak *et al* have reported the effect of point defects on structural, optical and electrical properties of Ga_2O_3 thin films [54]. They have investigated that Lorentzian width of thin films grown at varying oxygen pressure shows a minimum value at intermediate pressure. Variation of Lorentzian width with oxygen growth pressure is shown in figure 4(a). Hence, an intermediate oxygen growth pressure is required to grow high quality β-Ga_2O_3 thin films. Authors also evaluated that high density of point defects led to Fermi level pinning in thin films. Similar kind of work has been reported in the other

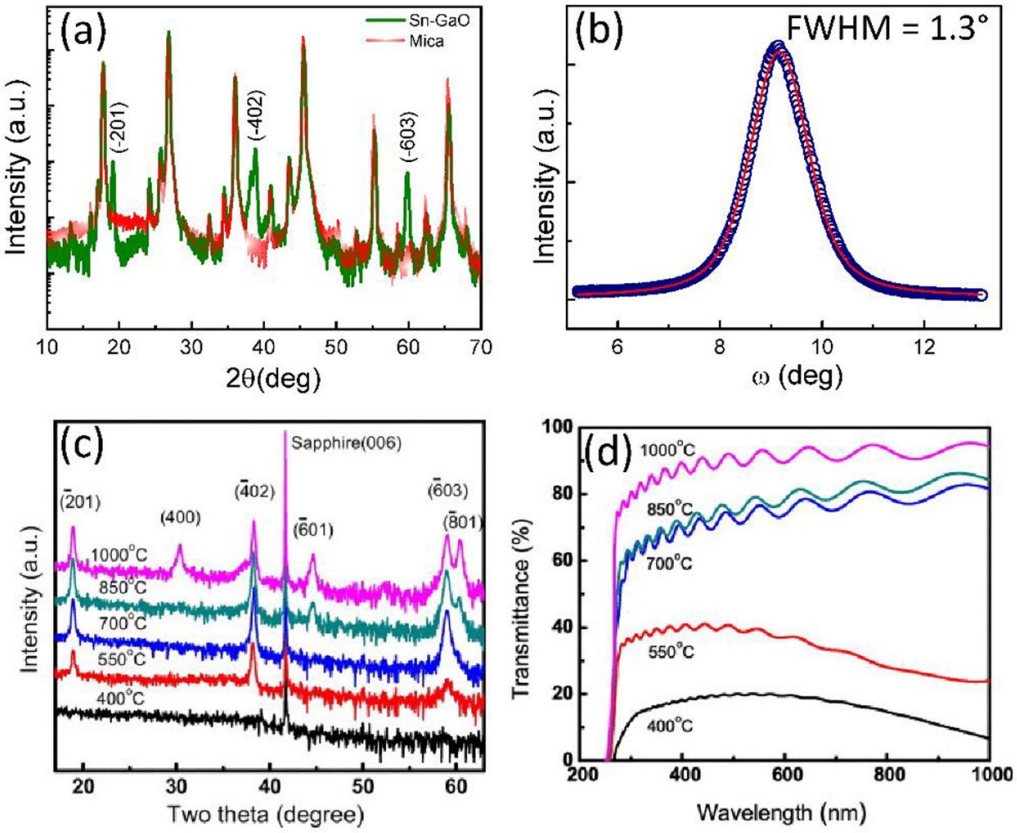

Figure 3. (a) XRD 2θ-scan of flexible β-Ga_2O_3/muscovite epitaxial film grown by PLD and (b) rocking curve of ($\bar{2}01$)-plane of β-Ga_2O_3 thin film. Reproduced from [53]. CC BY 4.0. (c) XRD patterns and (d) transmittance spectra of the Ga_2O_3 films grown on *c*-plane sapphire substrate at various substrate temperatures (400 °C–1000 °C). Reprinted from [140], Copyright (2012), with permission from Elsevier.

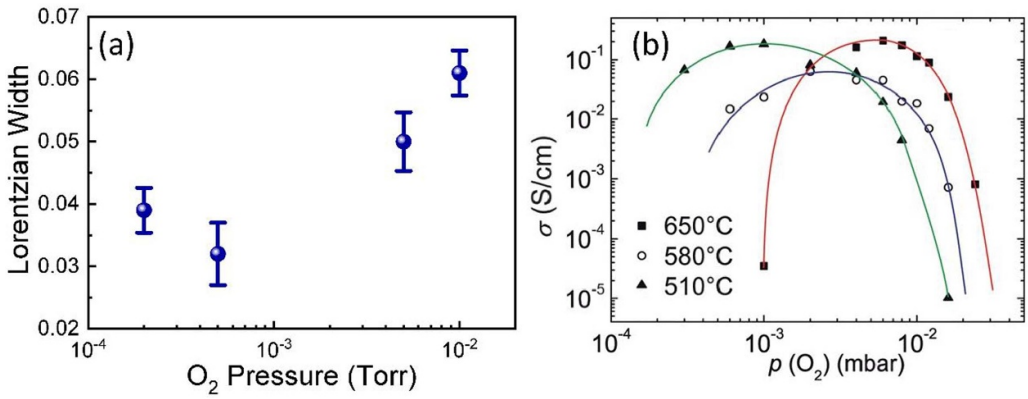

Figure 4. (a) Variation of Lorentzian width in UID β-Ga_2O_3 ($\bar{2}01$) films as a function of oxygen pressure, displaying relative change in point defects. The high-quality films were grown at intermediate growth pressure condition. Reprinted from [54], Copyright (2019), with permission from Elsevier. (b) Conductivity of Si-doped β-Ga_2O_3 with oxygen growth pressure for different growth temperatures. [141] John Wiley & Sons. Copyright © 2014 WILEY-VCH Verlag GmbH & Co. KGaA, Weinheim.

articles where a maximum conductivity of Si-doped Ga_2O_3 thin films were achieved at intermediate oxygen growth pressure as well as growth temperature as shown in figure 4(b) [138, 141].

Earlier, the variation in conductivity has been investigated by Orita *et al* in the case of Sn doped Ga_2O_3 thin films [142]. They suggested that the decrease in conductivity was due to phase change from β-phase to ε-phase of Ga_2O_3. The conductivity of 5 mol% SnO_2 doped β-Ga_2O_3 thin films was about 8.2 S cm^{-1}. Goyal *et al* studied the annealing effect on β-Ga_2O_3 thin films grown by PLD [143]. They found an increase in bandgap with increasing annealing temperature and they suggested that diffusion of Al content from sapphire to Ga_2O_3 increases with increasing substrate temperature which resulted in bandgap tuning. Authors observed highest bandgap of 5.15 eV for the films annealed at 1000 °C for 36 h.

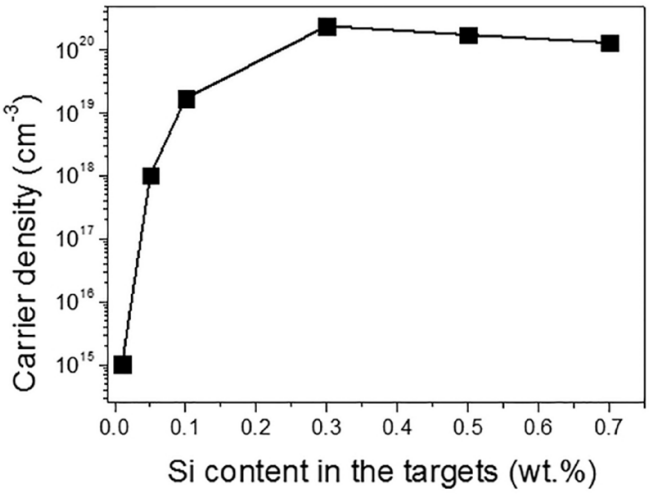

Figure 5. Carrier density in the films with <1% Si content variation in PLD target of β-Ga_2O_3. Reprinted from [144], with the permission of AIP Publishing.

Consequently, these annealed films can be used for deep UV device applications.

There are few reports related to the doping aspect of β-Ga_2O_3 thin films grown using PLD technique. Stefan *et al* measured the conductivity of ($\bar{2}01$) oriented monoclinic Ga_2O_3 thin films with 1 wt% SiO_2 content grown on *c*-sapphire [141]. The maximum conductivity of 0.2 S cm^{-1} was obtained for the films grown at 650 °C substrate temperature with 6×10^{-3} mbar oxygen pressure. However, in [145], Zhang *et al* have obtained the highest conductivity of about 2 S cm^{-1} for 1.1 at% Si-doped film. The observed carrier density of this film was 9.1×10^{19} cm^3. The decrease in carrier density was observed for further increment in Si doping. In the later work, authors demonstrated variation of carrier concentration of Si-doped Ga_2O_3 films by precisely varying Si content less than 1% in the target [144]. The variation of carrier density in Si-doped Ga_2O_3 is depicted in figure 5. The Si was observed to be an efficient dopant in Ga_2O_3 material to achieve carrier density up to 10^{20} cm^{-3}.

Later on, Zhang *et al* investigated the effect of Indium (In) doping on Ga_2O_3 thin films on *c*-plane sapphire [146]. They found two phases i.e. monoclinic and cubic of Ga_2O_3 corresponding to In content between 0.16 at% and 0.33 at%. The bandgap engineering of these films from 3.8 to 5.1 eV was achieved by tuning In content in the films as plotted in figure 6(a). Stable In doping in κ-$(In_xGa_{1-x})_2O_3$ was achieved up to $x = 0.28$ by Kneiß *et al* and further increase in In content resulted in phase segregation [148]. Hassa *et al* deposited κ-$(Al_xGa_{1-x})_2O_3$ with Al content $0.7 \leqslant x \leqslant 0.45$ and corresponding bandgap was engineered from 5.03 to 5.85 eV [136]. In case of β-phase, the maximum bandgap of 5.75 eV was reported with 0.53% Al content [147]. The variation in optical bandgap of Al doped Ga_2O_3 is depicted in figure 6(b). Wakabayashi Ryo *et al* demonstrated the effect of oxygen radical atmosphere for PLD deposited β-$(Al_xGa_{1-x})_2O_3$ films on (010) oriented β-Ga_2O_3 substrate [149]. It was found that heterostructures based on β-Ga_2O_3 could be fabricated more efficiently using oxygen radical assisted PLD rather than conventional oxygen atmosphere.

In case of rare earth doping, Wellenius *et al* demonstrated Eu doping in β-Ga_2O_3 thin films on the sapphire substrate with a substrate temperature of 850 °C [150]. They reported 5 mol%–10 mol% optimized Eu doping in Ga_2O_3 thin films for optoelectronic device applications. These films were polycrystalline, while, Chen *et al* successfully deposited ($\bar{2}01$) oriented Ga_2O_3 thin films with maximum Eu doping of 1.2 at% even at a low temperature of 500 °C [151]. Further, authors reported the effect of Er doping on the properties of β-Ga_2O_3 on the sapphire substrate. The enhancement of Er content in β-Ga_2O_3 led to shifting in diffraction peaks to the lower angle. It was suggested that shifting was attributed to an increase in the lattice constant because Ga^{+3} had smaller ionic radii than Er^{+3}. It was observed that surface roughness increased with an increase in Er doping into the films. Authors observed the highest roughness of thin film below 9 nm and it was clearly obvious that the film surface was smooth. Bandgap of the films decreased from 4.96 eV for an undoped film to 4.77 eV for Er doping of 7 at%. The reduction in band gap was attributed to the appearance of new unoccupied electron states (Er ions sitting at substitutional sites of Ga_2O_3) below the conduction band. The transmission spectrum having sharp absorption edge at 250 nm was observed, which shifted toward longer wavelength side with increasing Er content. Moreover, a few other reports are also available related to the growth of β-Ga_2O_3 thin films using PLD and are used for different applications [152–158].

3.2. MBE

The precise control over growth parameters under an UHV condition is the main advantage of MBE growth. Different type of devices such as FETs, photodetectors and Schottky diodes are reported on MBE grown Ga_2O_3 films [14, 159–162]. Two-dimensional electron gas (2DEG) has also been demonstrated in β-$Al_xGa_{1-x}O_3/Ga_2O_3$ heterostructures using this growth technique which is useful for the fabrication of high performance FETs [163].

Growth kinetics of Ga_2O_3 thin film deposition using plasma assisted MBE is displayed as a function of growth temperature (T_G) in figure 7 [164]. The symbols $\Phi_{Ga,}$ Φ_O and r_{Ga} were defined as Ga flux, oxygen flux and ratio of Ga to O respectively. Authors proposed that the MBE growth is governed by competition between volatile Ga_2O desorption and Ga_2O_3 accumulation. At high T_G and r_{Ga}, volatile Ga_2O desorption is more favored which results in lower growth rates. The growth diagram (GD) provided a growth window for MBE of Ga_2O_3 films.

In the beginning, Wong *et al* observed a parasitic conduction in the MOSFET devices fabricated on MBE grown Ga_2O_3 epilayer [165]. The epilayer was grown at 560 °C on Fe-doped β-Ga_2O_3 (010) substrates. Using secondary ion mass spectroscopy, it was observed that the epilayer interface possesses unintentional silicon concentration of 10^{19} cm^{-3}. Further, the reduction in Si content was performed by heating the substrate above 650 °C. Seven orders of reduction in leakage current

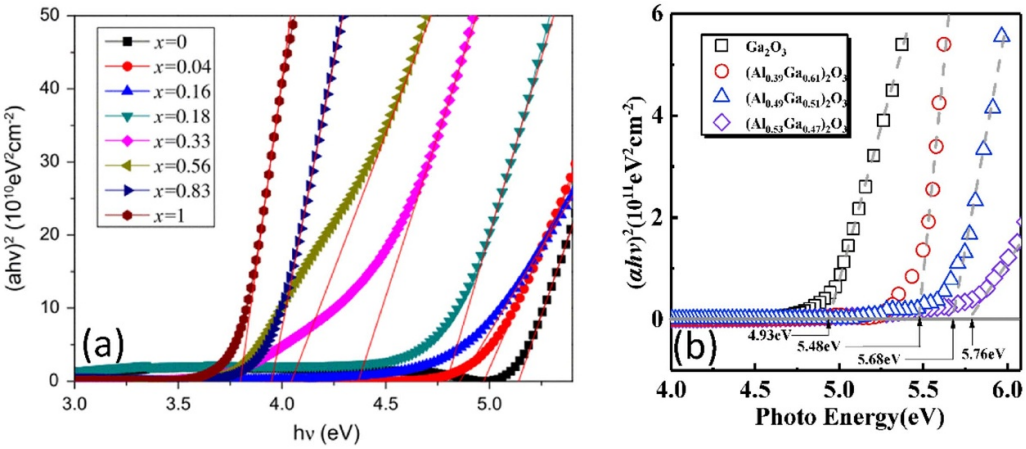

Figure 6. $(\alpha h\nu)^2$ versus $h\nu$ plot of (a) β-$(Ga_xIn_{1-x})_2O_3$ films with variation of indium contents from $x = 0$ to $x = 1$ and β-$(Al_xGa_{1-x})_2O_3$ films with varying Al content up to $x = 0.53$. Reprinted from [146], Copyright (2014), with permission from Elsevier. (b) The wide bandgap engineering is achieved from 3.8 to 5.75 eV using In and Al doping in PLD films. Reprinted from [147], Copyright (2018), with permission from Elsevier.

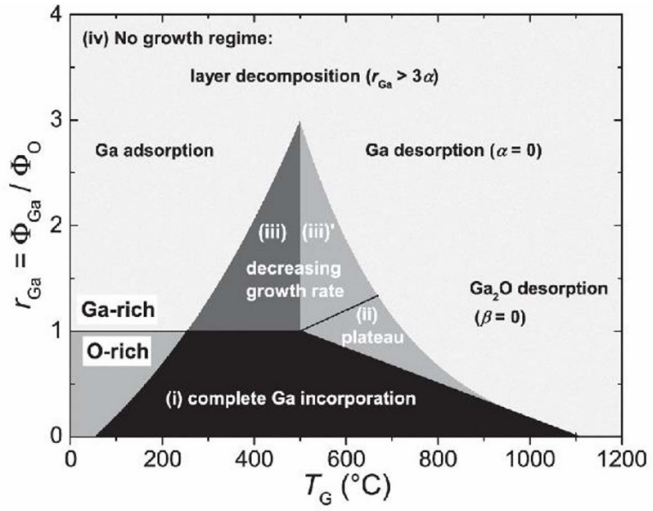

Figure 7. A GD for the Ga_2O_3 MBE growth including all experimental parameters (Φ_{Ga}; Φ_O) and T_G. It is divided into two major regimes: O-rich and Ga-rich. The GD illustrates regimes of complete (i), partial (ii), (iii), (iii′), and no Ga-incorporation (iv) as a function of T_G and r_{Ga}. Reprinted from [164], with the permission of AIP Publishing.

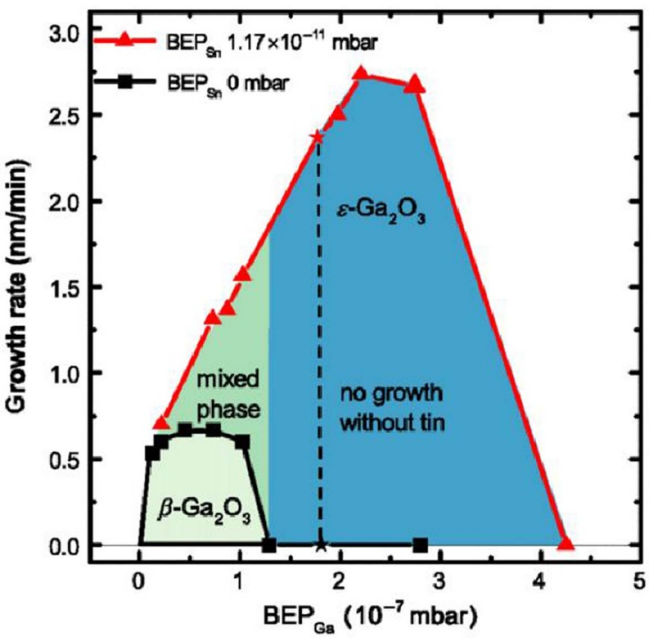

Figure 8. Comparison of the growth rates of series B (red triangles) and A (black squares) as a function of beam equivalent pressure $(BEP)_{Ga}$. No Sn was supplied in series A, whereas, 1.17×10^{-11} mbar BEP_{Sn} was used in series B. An attenuation of etching and an expansion of growth window with the presence of tin is observed. Reprinted (figure) with permission from [168], Copyright (2017) by the American Physical Society.

was observed for high temperature treated MOSFETs. High temperature treatment possibly resulted in either reduction in Si activation or charge compensation at the interface. Ahmadi *et al* have suggested a different approach to reduce the interface dopants [166]. They performed Ga polishing of substrate to reduce the Si content at the interface. However, Asel *et al* identified that Si dopant cell and RF oxygen plasma are the major sources of unintentional Si-doping [167]. The effect of dopant cell can be lessened by reducing the cell temperature when system is idle. Further, decreasing plasma power also resulted in lower background Si-doping. In another report, the reduction in SiO flux with decreasing Si-cell temperature is also reported [114].

Other than the β-phase, growth of ε-Ga_2O_3 has also been achieved using MBE method [168]. Kracht *et al* proposed the phase diagram as a function of BEP of Ga and Sn source which shown in figure 8. The metal (Ga and Sn) rich environment is favorable for ε-phase growth. Authors suggested that the presence of Sn in Ga_2O_3 may promote more octahedral Ga position which stabilizes the ε-phase. The growth of α-Ga_2O_3 thin films on *a*-plane sapphire substrate was also reported [169].

In 2013, Higashiwaki *et al* reported on growth of Ga_2O_3 thin films using the MBE technique for power device applications [32]. Figure 9(a) revealed morphologies of Ga_2O_3 thin

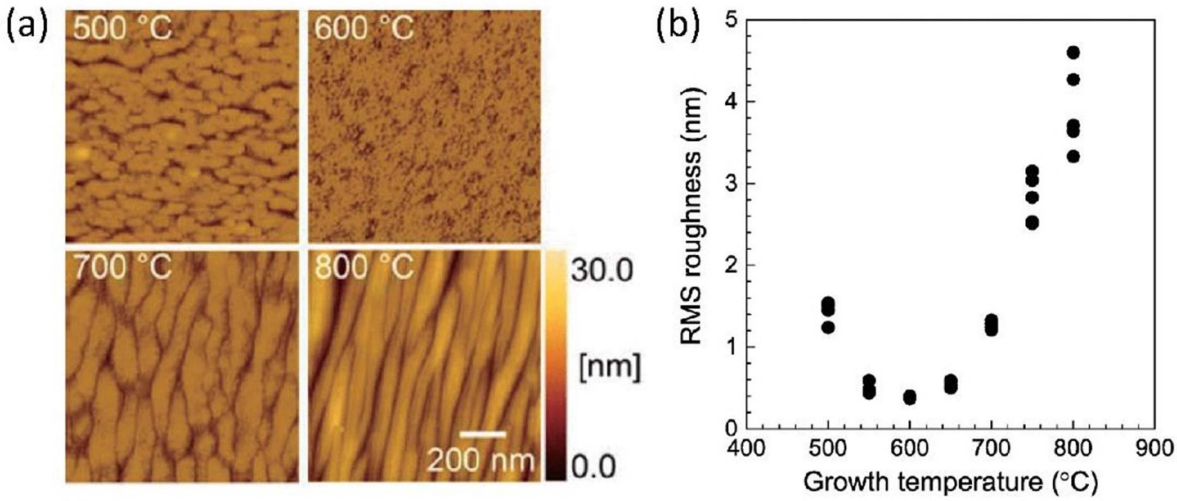

Figure 9. (a) Surface morphologies MBE Ga_2O_3 thin films grown at various temperatures and (b) RMS surface roughness of the Ga_2O_3 film as a function of growth temperature (500 °C–800 °C). The films grown at 550 °C–650 °C showed lowest roughness (<1 nm). [32] John Wiley & Sons. Copyright © 2013 WILEY-VCH Verlag GmbH & Co. KGaA, Weinheim.

film at various temperatures range 500 °C–800 °C. Figure 9(b) showed RMS roughness of Ga_2O_3 thin film at various temperatures range 500 °C–800 °C. Authors found the smoothest films at growth temperatures of 550 °C–650 °C.

Further, Yu *et al* deposited Ga_2O_3 thin films on GaAs (001) substrates at a temperature of 420 °C–450 °C using MBE [170]. The as-grown films were amorphous in nature. The RMS roughness was found to be about 2 and 3 Å. The Ga_2O_3–GaAs interface was found atomically flat. Guo *et al* have deposited ($\bar{2}01$) oriented β-Ga_2O_3 thin films on *c*-sapphire by laser MBE [160, 171]. In [160], they measured grain size of 150 nm film which is deposited at 5×10^{-3} Pa and 750 °C. The RMS roughness of thin film was about 3.42 nm. In addition, bandgap of 5.02 eV was observed for the film from UV absorption spectrum. A sharp absorption edge at 254 nm indicated that the photodetector fabricated from this film can be used for solar blind photodetectors.

The effect of buffer layers on MBE growth of β-Ga_2O_3 thin films were also investigated [161, 172]. Liu *et al* deposited (−201) oriented β-Ga_2O_3 thin films on *c*-sapphire with the homo-self-template buffer layer. They noticed enhancement in the crystal quality of film with buffer layer treatment. The FWHM of rocking curve decreased from 1.9° to 0.9° by applying buffer layer. A photodetector was fabricated using this film. The observed dark current and photoresponsivity were 0.04 nA and 259 A W^{-1}, respectively. This device had a quantum efficiency of 7.9×10^4% at the bias voltage of 20 V. Recently, the homoepitaxial growth of β-Ga_2O_3 on different substrate orientations that is (001), (010), (100) with 6° offcut and ($\bar{2}01$) were investigated by Mazzolini *et al* [55]. The growth rate, crystalline quality and surface roughness was studied. The growth rate was found to increase with respect to surface free energy enhancement of different orientations that follows: $\Gamma(100) < \Gamma(\bar{2}01) < \Gamma(001)$ and $\Gamma(010)$. In other report, Cheng *et al* investigated the growth mode evaluation on homoepitaxial β-Ga_2O_3 (100) substrates [173]. Researchers have found 2D layer by layer growth of (100) planes which makes this orientation a good candidate for 2D electronics.

Various doping elements such as Si, Al, Zn, In Ge, Mn and Fe have been realized to engineer the electrical and optical properties of Ga_2O_3 films using MBE [114, 147, 166, 174–176]. Kaun *et al* deposited Al-doped β-Ga_2O_3 thin films on (010) oriented β-Ga_2O_3 substrates by plasma-assisted MBE [162]. The β-Ga_2O_3 phase was stable for Al content less than 18% at 600 °C substrate temperature. This heterostructure grown at 650 °C demonstrated a sharp interface. Recently, α-$(Al_xGa_{1-x})_2O_3$ thin films on *m*-plane sapphire were grown using MBE to achieve full span bandgap by tunning Al content [80]. Authors reported that no phase segregation with Al doping ($0 \leqslant x \leqslant 1$). The optical bandgap of thin films was also investigated and found to vary from 5.4 to 8.6 eV. In-doped Ga_2O_3 thin films were deposited by Oshima *et al* on *c*-sapphire [175]. They noticed that these films are ($\bar{2}01$) oriented for Ga_2O_3 doped up to 35% In content. The bandgap of these films could be tuned from 5 eV to 4 eV with enhanced In content. The low temperature growth was preferable for lesser phase separation. In a more recent study by Ahmadi *et al*, investigations on Ge doped β-Ga_2O_3 thin films using plasma-assisted MBE has been carried out [175]. The authors obtained highest mobility of 97 cm^2 V^{-1} s^{-1} corresponding to carrier concentration of 1.6×10^{18} cm^{-3}. The mobility was double than the Sn-doped film with same carrier concentration. In another report [177], Zhao *et al* deposited Zn doped β-Ga_2O_3 thin films via MBE. The authors found shrinkage of the bandgap with increasing Zn concentration. They have also fabricated photodetector based on these doped thin films. The unintentional extra charge carriers induced by oxygen vacancies can be suppressed by doping of valence change element Mn in Ga_2O_3 as reported by Guo *et al* [178]. They observed two orders of enhancement in the resistance of Ga_2O_3 thin films after incorporation of Mn ions. XPS measurement of the O 1S peak showed that the oxygen vacancy peak got reduced

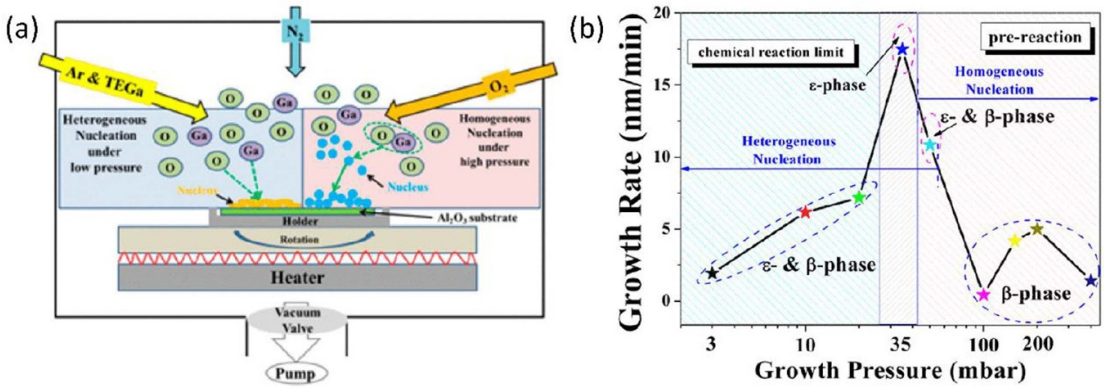

Figure 10. (a) Schematic illustration of homogeneous nucleation under low pressure and heterogeneous nucleation under high pressure in MOCVD system, homogeneous nuclei are formed above the substrate in vapor phase but heterogeneous nuclei are formed on the surface of substrate; (b) growth rate, crystal phase and nucleation change with respect to growth pressure. Pure ε-phase was obtained at 35 mbar and pure β-Ga_2O_3 was grown above 100 mbar pressure. Reprinted with permission from [188]. Copyright (2018) American Chemical Society.

after Mn doping. Hence the semi-insulating Ga_2O_3 could be grown by Mn doping. They also demonstrated that MSM photodetectors based on Mn-doped Ga_2O_3 have a much faster photoresponse time than bare Ga_2O_3. Similarly, Fe doping has also been investigated to obtain semi-insulating Ga_2O_3 films [176].

3.3. MOCVD

In recent years, there are some research groups around the world that are working towards the growth of Ga_2O_3 thin film using MOCVD technique. The maximum growth rate of β-Ga_2O_3 films of about 10 μm h^{-1} is reported in the MOCVD system where showerhead was coupled very close to the substrate [179]. Such a high growth rate is favorable for industrial application of the material.

MOCVD growth of Ga_3O_3 thin films have been reported on different substrates to achieve different epitaxial orientations. Deposition of $(\bar{2}01)$ oriented β-Ga_2O_3 films was achieved on sapphire (0001), MgO (111) and homoepitaxial β-Ga_2O_3 $(\bar{2}01)$ single crystals [111, 180, 181]. However, β-Ga_2O_3 (100) growth was performed on various substrates such as GaN (0001)/sapphire, $MgAl_6O_{10}$ (100), gadolinium gallium garnet ($Gd_3Ga_5O_{12}$) (110), $KTaO_3$ (100) and $SrTiO_3$ (100) [115, 182–185]. The $(\bar{2}01)$ orientation was also reported on MgO (110) substrate [186]. Deposition of another important phase i.e. ε-Ga_2O_3 was obtained on 3C-SiC (111), 3C-SiC (001), GaN (0001) and sapphire (0001) as reported in the literature [119, 187]. The α-phase growth using MOCVD was only reported on sapphire (0001) substrate [101]. The change in substrates and their orientations was found to useful to grow different orientations of Ga_2O_3. Porsok *et al* obtained the α and β phase of Ga_2O_3 on *m*- and *c*-plane sapphire, respectively in liquid injected MOCVD reactor [101]. Authors found that the choice of growth pressure also influenced the phase selection. Relatively lower growth pressure was required for α-phase growth on *m*-plane than β-phase on *c*-plane sapphire.

The different phases can be grown using MOCVD by tailoring growth conditions like precursors, pressure and temperature. Zhuo *et al* have reported that growth of β and ε phases are the function of growth temperature and VI/III ratio [119]. Authors successfully obtained phase transition from β to ε phase by reducing both parameters. Similarly, Chen *et al* have grown pure β and ε phases of Ga_2O_3 by controlling the growth pressure at constant growth temperature of 500 °C [188]. The lower biaxial stress of ε than β phase with sapphire induced by lattice mismatch promotes ε-Ga_2O_3 growth at heterogeneous nucleation sites. The phase diagram as a function of growth pressure for both phases is shown in figure 10(b). The optimum growth pressure for pure phase ε-Ga_2O_3 was 35 mbar. The mix phase Ga_2O_3 at lower growth pressures (<20 mbar) was obtained due to β-Ga_2O_3 nucleation on carbon sites on the surface of substrate. At high growth pressures, nuclei formed in homogeneous vapor phase resulted in the most stable β-Ga_2O_3.

Recently, Sun *et al* have precisely controlled the α, β and ε phases of Ga_2O_3 by tuning HCl flow rate in MOCVD reactor and fabricated high performance solar-blind photodetectors based on these α and ε phases of Ga_2O_3 films [111, 189–191]. Authors have achieved almost three-fold increase in the growth rate of β-Ga_2O_3 by insertion of 5 sccm HCl flow in reactor. Further increase in HCl flow at 10 sccm promoted mix phase $\beta + \varepsilon$ growth and further transformed in pure ε-phase at 30 sccm. Later on, $\alpha + \varepsilon$ mix phase was obtained with continuous increase in HCl flow rate. The HCl flow rate dependent XRD of all the thin films is depicted in figure 11.

For the first time, in 1996, Battiston *et al* showed the growth of Ga_2O_3 thin films on alumina as well as TiO_2 substrates via MOCVD [42]. They used gallium trishexafluoroaeetylacetonate as a precursor in the presence of oxygen. The deposition temperature was 470 °C with a deposition rate of 0.7 μm h^{-1}. As grown Ga_2O_3 films were amorphous. The phase modification has been observed from 600 °C to 1000 °C. Thereafter, in a few reports, Kim *et al* have also prepared Ga_2O_3 thin films using MOCVD [192–195]. In [192], authors have grown

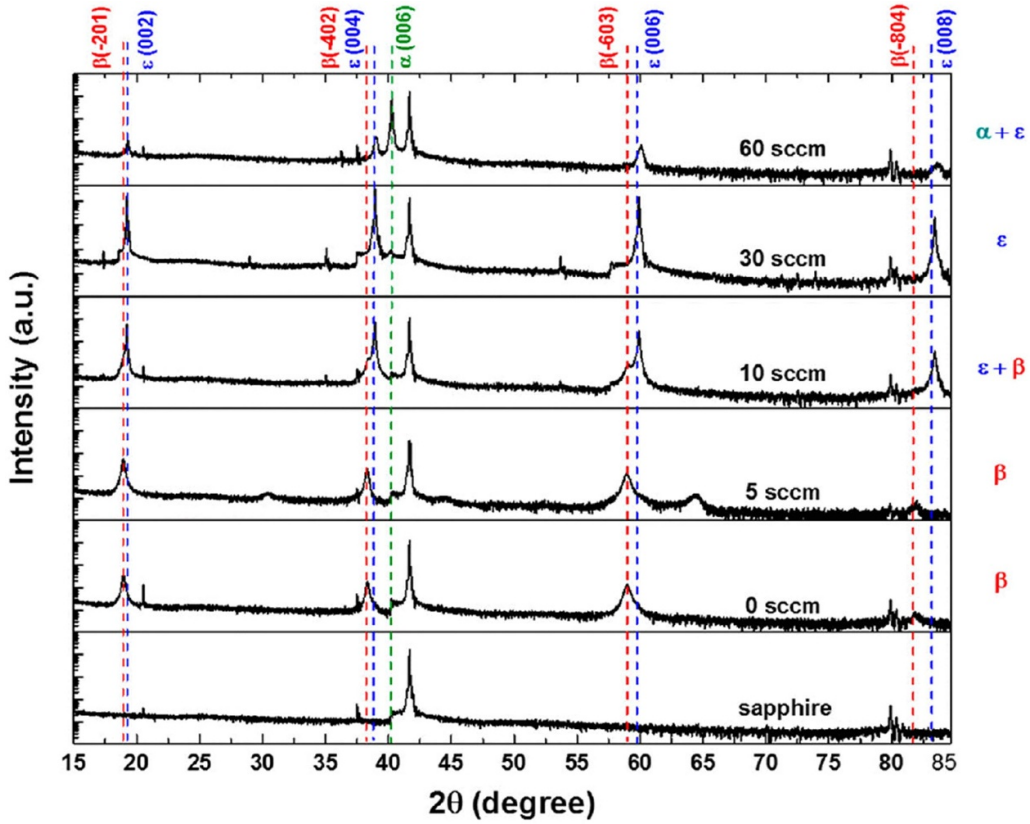

Figure 11. XRD patterns of Ga_2O_3 films grown under different flow rates of HCl. The β, ε and α phase was obtained with increasing HCl flow respectively. Reprinted with permission from [111]. Copyright (2018) American Chemical Society.

Ga_2O_3 thin film on Si (100) substrates and utilizing gallium isopropoxide, as a single precursor.

In [193, 194], Kim *et al* showed growth of Ga_2O_3 thin films on sapphire substrates using the same technique, and this time they used trimethylgallium (TMGa) as gallium precursor. The reaction was simply between TMGa and oxygen precursors. They have also investigated the effect of deposition temperature (750 °C–1050 °C) on structural and morphological properties of thin films using plan-view and cross-sectional scanning electron microscopy, XRD analysis, and atomic force microscopy (AFM). The RMS surface roughness of as-deposited and 1050 °C annealed Ga_2O_3 films were 1.15 and 2.28 nm, respectively. The AFM analysis indicates that RMS surface roughness increased by increasing the annealing temperature. In addition, Photoluminescence (PL) measurement revealed that the emission intensity in blue-green and UV region becomes stronger by the thermal annealing. Cho *et al* have reported the growth of β-Ga_2O_3 thin films using a new volatile source such as dimethylgallium isopropoxide for ALD and MOCVD technique [195]. MOCVD growth temperature was in the range of 450 °C–625 °C with reacting gas. In their studies, they used Si (001) substrates to grow thin films. In another article, Lv *et al* also studied the growth and characterization of β-Ga_2O_3 thin films on sapphire (0001) at different substrate temperatures by MOCVD [196]. They also used trimethylgallium (TMGa) and pure oxygen/water as precursors for gallium and oxygen, respectively.

Recently, Guo *et al* studied the growth characteristics and device properties of MOCVD derived β-Ga_2O_3 films [197]. They investigated the effect of growth temperature on structural, morphological, and optical properties of the thin film. It was noted that the $(\bar{2}01)$ peak intensity increased with increasing temperature which indicates the improvement in crystalline quality of β-Ga_2O_3 films. The optical band gap was found within 4.8–4.9 eV at various growth temperatures.

In recent years, Mi and his co-workers have reported various studies related to the growth of undoped and doped β-Ga_2O_3 films using MOCVD and MOVPE techniques [180, 183, 186, 198–206]. In [198], the authors have investigated Sn doping in β-Ga_2O_3 films with different tin concentrations which were grown on MgO (110) substrates by MOCVD at 700 °C. Effect of Sn doping on the structural, electrical, and optical properties of films was investigated. The cross sectional HRTEM and SAED image displayed in figure 12(a) confirms the β-Ga_2O_3 (100)||MgO (110) with β-Ga_2O_3 (201)||MgO (111) relationship. It was observed that 10% Sn doped film exhibited the best electrical conductivity properties with the lowest resistivity about 5.21×10^{-2} Ω cm. This resistivity was ten orders of magnitude lower as compared to the undoped film as shown in figure 12(b). The optical transmittance spectra for Sn doped β-Ga_2O_3 film as a function of wavelength in the range of 200–800 nm are shown in figure 12(c). The average transmittance of all the films in visible rage exceeded 87%. The bandgap of these Sn-doped

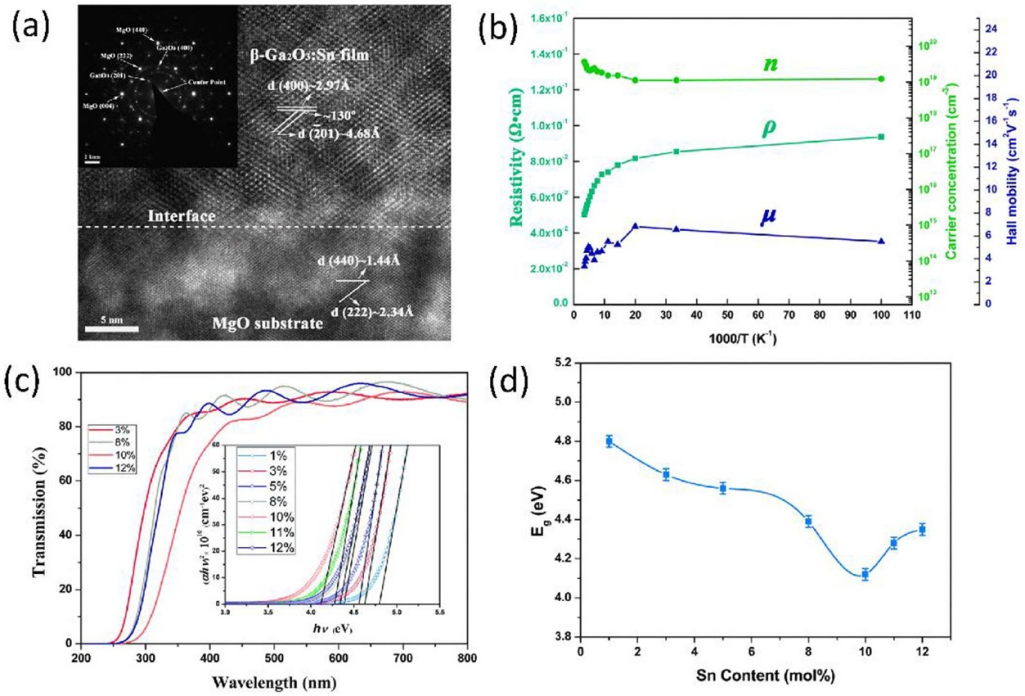

Figure 12. (a) Cross-sectional HRTEM and SAED micrographs of the interface between 10% Sn-doped β-Ga_2O_3 film and the MgO substrate. (b) Resistivity (r), carrier concentration (n) and Hall mobility (m) of β-Ga_2O_3 films with 10% Sn doped as a function of reciprocal temperature. (c) The optical transmittance spectra of β-Ga_2O_3:Sn samples. The plot of $(\alpha h\nu)^2$ as a function of photon energy $h\nu$ are shown in the inset (d) E_g of the β-Ga_2O_3:Sn films as a function of Sn content. (a)–(d) Reproduced from [198] with permission of The Royal Society of Chemistry.

Ga_2O_3 thin films was tuned between 4.1 and 4.8 eV which is depicted in figure 12(d).

3.4. Sputtering

Sputtering is a physical vapor deposition technique in which atoms are ejected from the target material by positively charged ions. The momentum transfer mechanism is responsible for ejection of atoms from the material. In the case of magnetron sputtering, magnetic field is used to create plasma at a lower pressure as compared to a normal sputtering process. Generally, Ar or mixture of Ar and O_2 ambient is utilized for the deposition of β-Ga_2O_3 thin films. In addition, the pre-sputtering of target is required to remove the target contamination from film.

The crystalline quality of sputter deposited thin films depends on growth temperature, sputtering power and growth pressure of the chamber. Effect of sputtering power on structural, optical and morphological properties were studied by Li and coauthors [207]. The crystalline quality of β-Ga_2O_3 films were improved with increasing sputtering power from 160 to 200 W. Figure 13 shows the FWHM and peak intensity of ($\bar{4}02$) plan as a function of sputtering power. A red shift in the blue and green emission of PL spectra was also observed with increase in sputter power. This red shift was ascribed to enlarged grain size in the films. Shurig *et al* also optimized all the growth parameters to obtain stoichiometric Ga_2O_3 thin films [208]. Authors found that the refractive index got highly deviated for the case of nonstoichiometric

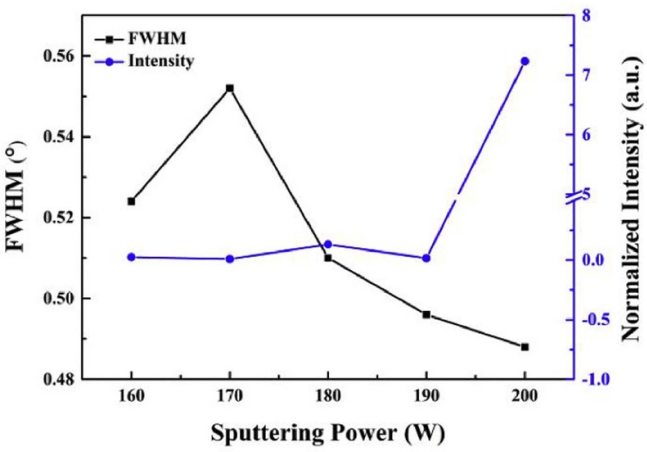

Figure 13. β ($\bar{4}02$) peak intensity and FWHM as a function of sputtering power displays improvement in crystalline quality of film. Reprinted from [207], Copyright (2018), with permission from Elsevier.

films which is useful information to tailor antireflecting phenomenon in Ga_2O_3. The sputtering growth of Ga_2O_3 thin films have been grown on various substrates like Si (100), GaN, sapphire (0001), MgO (100), $MgAl_2O_4$ (100) and SiC (6H) [113, 117, 209, 210]. MgO (100) substrate possesses lowest lattice mismatch with β-Ga_2O_3. The structural and optoelectronic properties of Ga_2O_3 thin films on multilayer substrates such as ITO (indium tin oxide)/quartz glass [211, 212], Cu/ITO/polyethylene terephthalate [213], SiO_2/Si [214],

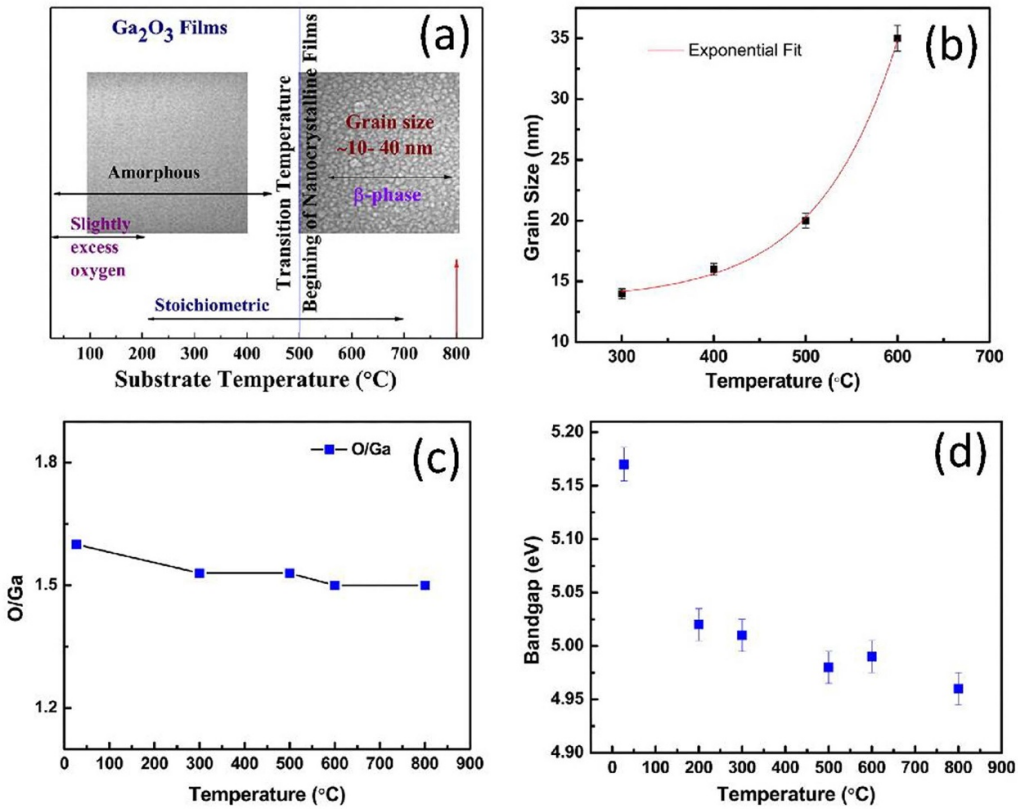

Figure 14. (a) Phase diagram summarizing the microstructure evolution of Ga_2O_3 films as a function of temperature. (b) Variation of grain size of Ga_2O_3 films with substrate temperature. (c) Variation of oxygen to gallium ratio in the Ga-oxide films as a function of Ts. The ratio was determined from RBS measurements. Slightly higher values than expected for films grown at RT indicate excess oxygen in the films. (d) Variation of bandgap with Ts for Ga_2O_3 films. (a)–(d) Reprinted with permission from [218]. Copyright (2013) American Chemical Society.

CIGS soda-lime glass [215], Cu_2O_3/ITO/quartz glass [216] were also investigated. The effect of homo buffer layer on growth of β-Ga_2O_3 thin films were studied [210]. The use of high temperature (700 °C) grown buffer layer resulted in crystallinity improvement of films. Authors also reported that photodetectors fabricated on films with buffer layers demonstrated relatively high performance than films without buffer layer.

In [211], Jianjun *et al* observed that the thickness of ITO film in Ga_2O_3/ITO structure tuned the electrical and optical properties. The low sheet resistance of 323 Ω sq^{-1} and high transmittance of 77.6% was observed for β-Ga_2O_3 (50 nm)/ITO (23 nm) at 280 nm. In [212], Chengyang *et al* deposited the alternating multilayers of Ga_2O_3 (25 nm)/ITO (11 nm). They found the lowest sheet resistance of 225.5 Ω sq^{-1} and the highest transmittance of 62.9% at 300 nm wavelength for two periods with a thickness of 72 nm.

In one report, Shigetoshi *et al* studied the electrical and optical properties of β-Ga_2O_3 films (100 nm thick) on the sapphire (0001) substrate [217]. The substrate temperature and working pressure during deposition were kept at 500 °C and 0.03 Pa, respectively. The films with orientation of $(\bar{2}01)$ were obtained without an oxygen atmosphere. Further increasing oxygen pressure, polycrystalline Ga_2O_3 thin films were observed. The authors found the optical transmittance of as-grown films was more than 80%. In this study, the electrical resistivity was also measured. They obtained the resistivity of films with (0.03 Pa) and without oxygen pressure as 5×10^7 Ω cm and 2×10^3 Ω cm, respectively.

The growth temperature and pressure play a crucial role to deposit thin films. In 2013, Kumar *et al* prepared β-Ga_2O_3 thin films on Si (100) substrate using magnetron sputtering [218]. The authors varied substrate temperatures in the range of 25 °C–800 °C. It can be seen clearly that the as-deposited films are amorphous below 500 °C and has polycrystalline nature above 500 °C as shown in figure 14(a). Figure 14(b) shows an exponential incensement in the grain size with increasing substrate temperature. Stoichiometry of the film improved approaching the exact O/Ga ratio as shown in figure 14(c). A decrease in the bandgap of films was observed from 5.17 to 4.96 eV with enhancement in temperature (as depicted in figure 14(d)). In the most recent study by Akazawa *et al*, the effect of substrate and deposition ambient on crystal structure of Ga_2O_3 films was investigated [219]. Authors used different substrates such as *c*- and *a*-planes sapphire, and Si (100). When the deposition was performed under O_2 ambient, β-phase of Ga_2O_3 formed on Si (100) at 600 °C and *c*-sapphire at 300 °C whereas the films deposited on *a*-sapphire at 600 °C was obtained α-Ga_2O_3. However, deposition under H_2O vapors resulted in the appearance of γ-phase on *c*-sapphire and coexistence α and γ-phase on *a*-sapphire above

800 °C. The β-phase of Ga_2O_3 films were deposited on Si (100) under H_2O vapors.

In one report, effect of thickness on the crystalline quality of β-Ga_2O_3/SiO_2 thin films was carried out by Ishibashi *et al* [220]. They found that crystalline quality improved whereas absorption coefficient decreased with increasing the film thickness from 100 to 400 nm. In 2014, Ramana *et al* deposited Ga_2O_3 thin films of thickness about 40 nm on Si (100) substrate at the temperature ranging from 25 °C to 600 °C [221]. The Ga_2O_3 films deposited below 500 °C were amorphous. Further, increasing temperature above 500 °C resulted in the appearance of crystalline phase. The RMS roughness of these films increased from 0.5 nm to 3 nm with enhancement in substrate temperature. The stoichiometry of these films was in good agreement with Ga_2O_3, since gallium was in its highest chemical state (Ga^{+3}). Refractive index of these films also increased with temperature due to improvement in the crystal structure and packing fraction. The electrical resistivity of amorphous film grown at 300 °C was 200 Ω cm whereas the value for crystalline film grown at 600 °C was 1 Ω cm. A sharp decrease in resistivity was observed with the appearance of amorphous to the crystalline phase. In [214], Chang *et al* grew 800 nm thick Ga_2O_3 thin film on SiO_2/Si substrate. They found that the photocurrent for 900 °C annealed film at zero bias was three orders of magnitude larger than dark current. Authors suggested that these films could be a good photocathode for hydrogen generation due to its good thermal stability.

3.5. Mist CVD

Mist CVD is a simple and cost-effective growth method which uses ultrasonic transducers to create mist particle from the source. The gallium acetylacetonate is widely used as a gallium source [46]. These mist vapors are transferred in furnace using carrier gas where thin film growth takes place. The mist CVD is commonly used method to grow corundum structured α-Ga_2O_3. Currently, high crystalline quality growth of α-Ga_2O_3 on two-inch sapphire substrate have been achieved [222, 223]. In both the articles, different system designs were adopted to achieve large area growth. Kim *et al* have used rear flow to control the growth. The film thickness was varying from 400 to 800 nm in the wafer. However, Hao *et al* have used vertical hot wall mist CVD. The camera image of two-inch wafer is depicted in figure 15(a). Authors achieved highly uniform films with thickness variation less than 3% as shown in figure 15(b). The FWHM of (0006) plane was varying between 295 and 307 arcsec recorded at different points P1–P6 (figure 15(c)). The rocking curve of $(10\bar{1}4)$ is presented in figure 15(d) whose FWHM varied from 526 to 737 arcsec.

In 2008, Fujita *et al* reported the high quality α-Ga_2O_3 thin films using mist CVD [46]. The thin films grown at 470 °C substrate temperature showed FWHM of 60 arcsec. Authors suggested that both low temperature as well as unique growth method are responsible for stable α-phase growth. Recently, Uno *et al* have proposed the growth mechanism for α-Ga_2O_3 which is shown in figure 16 [58]. The oxygen atom in the α-phase was found to originate from water vapors. The formation

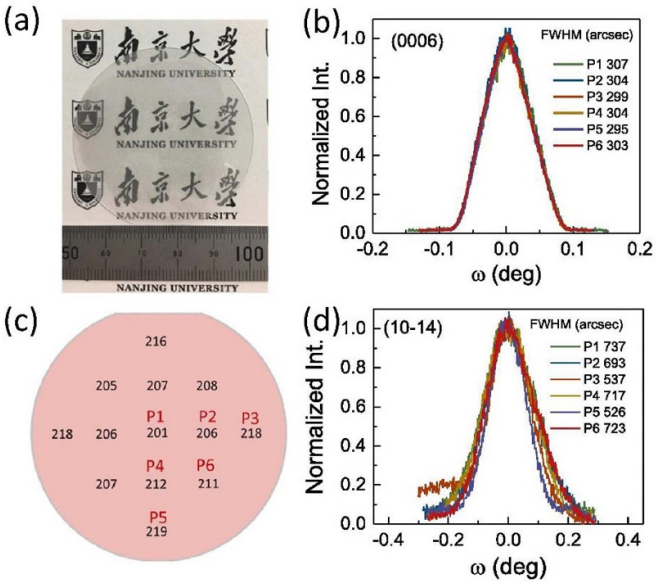

Figure 15. Photograph (a) and thickness distribution (b) of the α-Ga_2O_3 epilayer grown at 530 °C on two-inch sapphire substrate. (c) and (d) Showing the rocking curves of α-Ga_2O_3 (0006) and $(10\bar{1}4)$ planes, respectively, were recorded from six different points (P1–P6) as indicated in (b). (a)–(d) Reprinted from [223], Copyright (2020), with permission from Elsevier.

of thin film takes place via ligand exchange mechanism. The acetylacetone leaves as a ligand as depicted in step 4 of figure 16.

Other than the α-phase, β, γ, ε and κ-phases of Ga_2O_3 was also reported using mist CVD method [82, 127, 224, 225]. Lee *et al* have reported the enhanced thermal stability of α-Ga_2O_3 by Al doping [226]. Authors have used different Al composition to stabilize the α-phase at high temperatures. Figure 17 shows the transition temperature from α to β phase as a function of Al composition. A slight doping of Al ($x = 0.2$) in Ga_2O_3 films can enhance thermal stability of α-phase about 300 °C with a small change in the optical bandgap.

Despite growth temperature, the choice of substrate was also proven to control the different kind of phases of Ga_2O_3 in these reports. Oshima *et al* found that pure α and γ phases were grown on sapphire (0001) and $MgAl_2O_4$ (100) substrates respectively [82]. Authors reported the refractive index of about 2.0 and bandgap of 5.0 eV for γ-Ga_2O_3. The thermally stable ε-Ga_2O_3 up to 800 °C was achieved on *c*-plane AlN substrates by Tahara *et al* [225]. Nishinaka *et al* investigated the crystal structure of ε-Ga_2O_3 films grown on GaN (0001) and $SrTiO_3$ (111) templates [127]. In another report, authors have used α-Fe_2O_3 buffer layer to grow α-Ga_2O_3 on *a*-, *m*-, and *r*-plane sapphire substrates [227]. Authors have also achieved real breakthrough results in successfully growing single domain κ-Ga_2O_3 thin films using mist CVD [51]. The atomically flat single domain films were facilitated due to isostructural FZ grown ε-$GaFeO_3$ substrates. The in-plane rotational domains were absent in the x-ray ϕ-scan which confirms the single domain of κ-phase. Jinno *et al* have used α-$(Al_{0.4}Ga_{0.6})_2O_3$ buffer layer to effectively control the ε and α

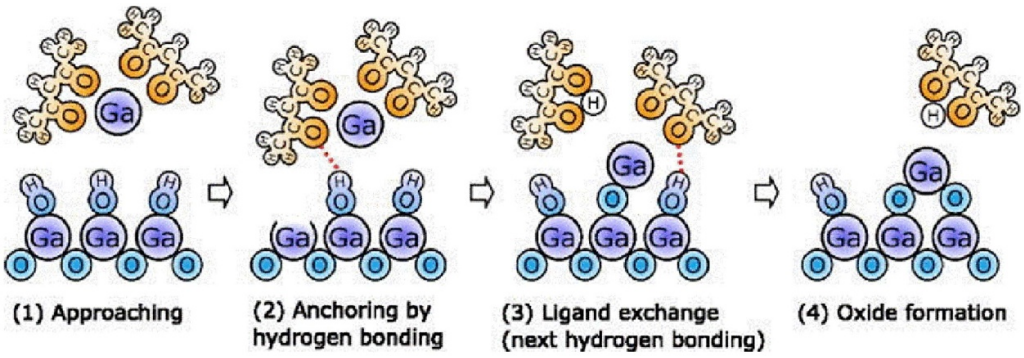

Figure 16. Proposed growth mechanism for α-Ga_2O_3 using mist CVD. Reprinted from [58], with the permission of AIP Publishing.

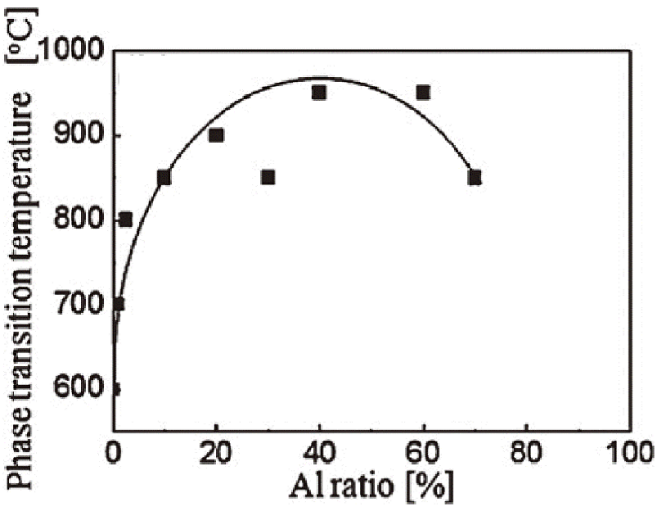

Figure 17. The temperature of phase transition to the β-phase as a function of Al ratio in the α-phase films. Reproduced from [226]. © 2015 The Japan Society of Applied Physics. All rights reserved.

Table 3. Different combination of precursors used for atomic layer deposition of Ga_2O_3 thin films.

Ga precursor	Oxygen precursor	References
Pentamethylcyclopentadienyl gallium ($GaCp^*$)	$H_2O + O_2$ plasma	[57]
Trimethyl gallium(TMGa)	H_2O	[187]
Trimethyl gallium (TMGa)	30% H_2O_2 with 70% H_2O	[232]
Trimethyl gallium (TMGa)	O_2 plasma	[108, 233–238]
Triethyl gallium (TEGa)	Dry oxygen	[239]
Tris(dimethylamino) gallium (III)	DI water	[240]
TMGa	Ozone	[241]
Dimethylgallium amide	Oxygen	[242]
Tris (2,2,6,6-tetramethyl-3,5 heptanedionato) gallium (III), (Ga(TMHD)3)	O_2 plasma	[243]

phases [224]. The lattice mismatch between buffer layer and α-phase was 2.2% while 1.2% in case of ε-phase. Authors have reported highly stable ε-Ga_2O_3 below 600 °C and α-Ga_2O_3 films above 600 °C. Shimazoe *et al* have epitaxially grown κ-Ga_2O_3 on $LiNbO_3$ (0001) and $LiTiO_3$ (0001) substrates [133]. Further, authors have used α-Fe_2O_3 buffer layer to grow α-Ga_2O_3 films on the same substrates.

The bandgap engineering of Ga_2O_3 films were reported using mist CVD. In-doping in the ε-Ga_2O_3 was performed by Nishinaka *et al* [92]. Authors have observed phase segregation for $x > 0.2$ in $(In_xGa_{1-x})_2O_3$ films. The optical bandgap was reduced from 5.0 to 4.5 eV by In incorporation up to $x = 0.2$. However, Ito *et al* have reported Al composition with $x = 0.81$ to grow α-$(Al_xGa_{1-x})_2O_3$ without phase segregation [228]. The optical bandgap was 7.8 eV corresponding to aforementioned Al composition. Electric properties of α-Ga_2O_3 were also tuned using Sn doping [229–231]. The maximum carrier concentration of 1×10^{20} cm^{-3} was achieved corresponding to 0.4% Sn in the source material [230]. Recently, Akaiwa *et al* have reported the maximum hall mobility of 65 cm^2 V^{-1} s^{-1} corresponding to 1.2×10^{18} cm^{-3} carrier concentration in α-Ga_2O_3 films grown on *m*-plane sapphire substrate [229].

3.6. ALD

In the ALD method, precursor gases are selected in such a manner that surface is passivated after the deposition of one atomic layer. Further, these passivated atoms must be removed before deposition of the next layer by various methods (chemical reactions, thermal spikes, etc). Therefore, ALD is a highly advantageous technique for control of film thickness up to one atomic layer with large area uniformity. Recently, Plasma-enhanced ALD (PEALD) is used to grow thin films which have the benefit of better-quality film deposition at a lower temperature than conventional thermal ALD system.

Various reported precursors for ALD growth of Ga_2O_3 thin films are shown in table 3. In one study, Ramachandran *et al* have used new precursors tris (2,2,6,6-tetramethyl 3,5-heptanedionato) gallium (III) $(Ga(TMHD)_3)$ as a gallium source and O_2 plasma as an oxidant for PEALD of Ga_2O_3 thin films [243]. They deposited amorphous Ga_2O_3 thin films on SiO_2/Si substrate at substrate temperature ranging from 200 °C to 400 °C. They have also studied thickness dependence on the number of reaction cycles without any nucleation delay at 200 °C.

It was observed that thickness varied linearly with the number of cycles as shown in figure 18(a). The growth rate was

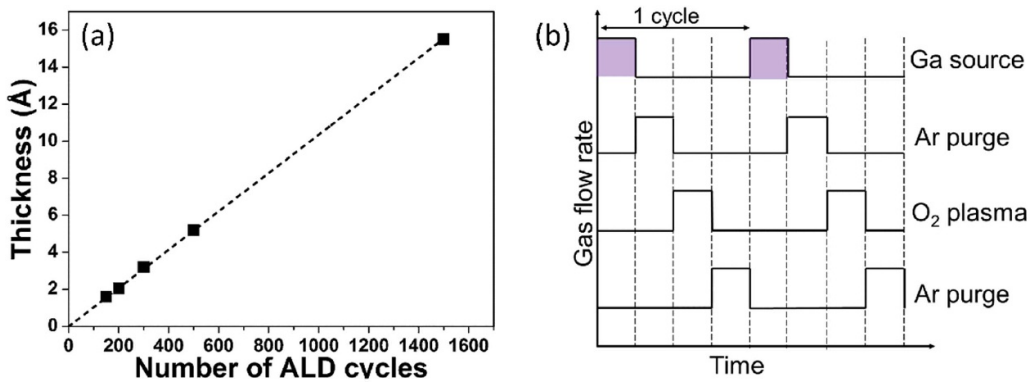

Figure 18. (a) Thickness of Ga_2O_3 films deposited at 200 °C on SiO_2/Si substrates versus the number of ALD cycles. Reproduced from [243] with permission of The Royal Society of Chemistry. (b) A schematic diagram of thin film deposition via ALD method. One deposition cycle consisted of four pulses: $((CH_2)_2GaNH_2)_3$ vapor pulse with 100 SCCM Ar carrier gas for 0.1 s, an Ar purge gas pulse for 2 s, an O_2 plasma gas pulse for 1 s, and an Ar purge gas pulse for 0.4 s. The period cycle was repeated until the desired thickness. Reprinted from [242], with the permission of AIP Publishing.

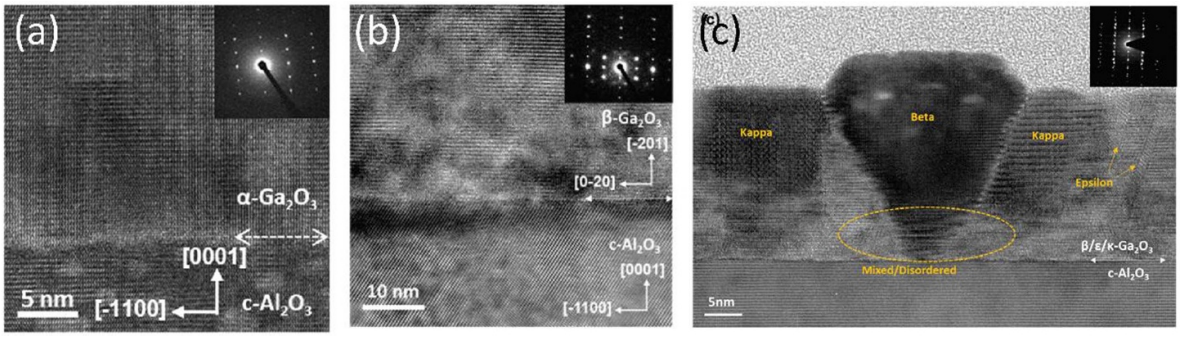

Figure 19. Cross-sectional (a) TEM and (b) SEAD (insets) of different phases of Ga_2O_3 deposited using ALD at the film-substrate interface. (c) Small area FFT across the high-resolution image was used to identifying the different phases for various grains. (a)–(c) Reprinted with permission from [108]. Copyright (2020) American Chemical Society.

constant during the complete process. These films showed RMS roughness in the range of 0.15–0.51 nm.

Shan *et al* have deposited Ga_2O_3 thin films on Si (100) and sapphire (0001) substrates using PEALD technique [242]. They have used two precursors such as dimethylgallium amide $((CH_2)_2GaNH_2)_3$ and O_2 plasma for the growth. During thin film growth, one growth cycle consisted of four pulses in sequence: $((CH_2)_2GaNH_2)_3$ vapor pulse with 100 sccm. Ar carrier gas for 0.1 s, an Ar purge gas pulse for 2 s, an O_2 plasma gas pulse for 1 s, and an Ar purge gas pulse for 0.4 s. These four pulses were defined as one deposition cycle. Figure 18(b) depicts a schematic diagram related to the deposition process. Thickness of film is controlled by the number of cycles. In their study, they used 1000 cycles on Si (100) and sapphire (001) substrates by PEALD. They observed significant improvement in the insulating properties of films with rapid thermal annealing at 700 °C and 900 °C for 1 min under O_2 atmosphere. The estimated bandgap of annealed thin films was in between 5.0 and 5.24 eV.

In their later studies, Shan *et al* have deposited amorphous Ga_2O_3 thin film on p-Si (100) [244–246]. In [244], authors have investigated the effect of different growth temperatures on the properties of thin films. They obtained bandgap of 5.0, 5.1, 5.3 eV at 50 °C, 150 °C, and 250 °C, respectively. In addition, the RMS roughness of thin films was 0.27, 0.20, 0.49 nm for growth temperature of 50 °C, 150 °C, and 250 °C, respectively. They have observed the decrease in dielectric constant of Pt/Ga_2O_3/Si structured thin film with a raise in temperature due to the formation of a low dielectric constant layer (SiO_2). In other reports [245, 246], authors prepared Ga_2O_3 and Ga_2O_3-Ti_2O_3 (GTO) nano mixed thin films using PEALD method and GTO films revealed improve dielectric constant than Ga_2O_3 thin films. In some recent works by Allen *et al* [247–249], trimethylgallium (TMGa) and $((CH_2)_2GaNH_2)$ were used as Ga source while oxygen plasma was used as an oxygen source for atomic layer deposition of thin films in PEALD. In [250], authors demonstrated the passivation of crystalline silicon (100) by Ga_2O_3 thin films. The effective passivation was observed with post annealing of samples at 350 °C for 180 min [243]. They have successfully demonstrated the uniform passivation for four-inch p-type and n-type Si wafers. The observed activation energy for passivation and de-passivation was 0.5 and 1.9 eV, respectively.

Recently, growth of different crystalline phases of Ga_2O_3 on *c*-plane sapphire have been reported using ALD [108, 239]. α, β, ε and κ phases were controlled using different parameters such as composition of plasma gas, gas flow, growth temperature and growth pressure [108]. The ε-phase was obtained with the β and κ phases. Crystal structure of all four phases were confirmed using TEM as shown in figure 19.

Table 4. Growth parameter dependent different phases of Ga_2O_3 thin films and their material properties. Reprinted with permission from [108]. Copyright (2020) American Chemical Society.

	β	α	ε (κ)
Growth temperature (°C)	295	295	⩾365
Growth pressure (mTorr)	⩽10	⩽10	⩾100
Gas type	Ar/O_2	O2	O2
Total gas flow (sccm)	5	40	100
XRD FWHM (arcsec)	268	250	2250
RMS roughness (nm)	0.3	0.1	1.0
Bandgap (eV)	4.8	5.0	4.8

All the phases dependent on these parameters are tabulated in table 4.

In a few reports, the post annealing effect under N_2 ambient on PEALD deposited Ga_2O_3 thin films were investigated by Altuntas *et al* [238, 251], Dezelah *et al* [252] and Donmez *et al* [253]. The β-Ga_2O_3 films were annealed at 700 °C, 800 °C, and 900 °C for 30 min which underwent the crystalline phase. Further, Altuntas *et al* have fabricated Al/β-Ga_2O_3/p-Si metal oxide semiconductor capacitors [238] and it was noticed that effective dielectric constant decreased whereas the leakage current improved with the increase in annealing temperature. In this study, they measured the oxide breakdown field for the PEALD grown β-Ga_2O_3 thin films and mentioned that its highest value than previously reported values. The highest reverse breakdown voltage about 18 MV cm^{-1} was observed for 800 °C annealed films. Post annealing effects on Ga_2O_3 films in oxygen atmosphere were also investigated [234]. The thin films annealed at 1000 °C for 2 h showed good crystalline quality with ($\bar{2}01$) preferred orientation. The bandgap of annealed film increased from 4.56 eV to 4.97 eV as compared to as grown film.

4. Summary and future perspectives

Currently the single crystal substrates are available for β-phase of Ga_2O_3 only. Therefore, thin film and epitaxial growth methods play important role for the development of research and technology of other phases of Ga_2O_3. In this review, recent advances on the development of the epitaxial growth of different Ga_2O_3 polymorphs, with an emphasis on growth methods such as PLD, MBE, MOCVD, mist CVD, sputtering and ALD are summarized. Figure 20 displays the radar chart of current research status of Ga_2O_3 polymorphs with respect to the epitaxial growth, availability of single crystal substrates, doping, physical properties and device applications. The widest circle indicates that the majority of research progress is made on the investigation of β-Ga_2O_3 phase. The α-phase Ga_2O_3 is being heavily studied well, mainly on the epitaxy rather on the bulk substrates.

It is also observed that the epitaxial growth of different polymorphs depends on growth conditions like temperature, pressure, carrier gas, III/V ratio, substrate as well as doping. Additionally, the phase changes of Ga_2O_3 were also highly related to growth technique/tool. Interestingly, the phase transition temperature can also be tuned by doping condition while the physical origin of doping induced phase stability requires further investigation.

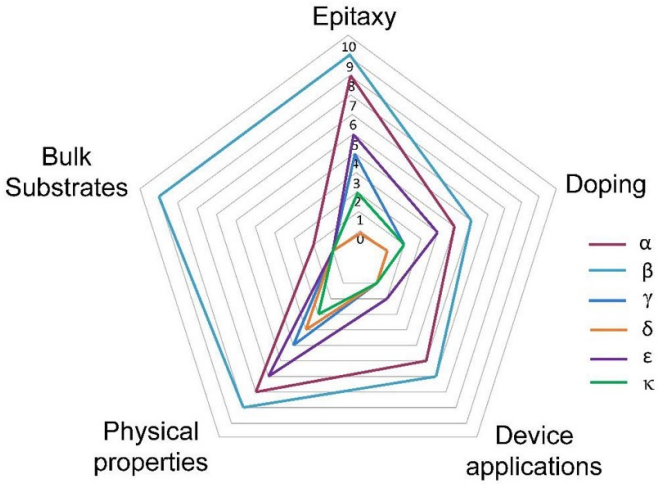

Figure 20. Radar chart of recent development status of Ga_2O_3 polymorphs with respect to availability of bulk substrates, exploration of physical properties and progress in epitaxial growth, doping and device applications.

Challenges, perspective and future opportunities:

(a) The majority of research on gallium oxide has been carried out on α and β phases. Thus, limited physical properties of other phases are known. Therefore, more efforts are needed to explore other phases of Ga_2O_3. The investigation of key physical properties such as electron mobility, effective mass, electrical and thermal conductivities are the need of the hour for future development of Ga_2O_3 technology. The existence of polarization in ε- and κ-Ga_2O_3 has been theoretically predicted but still not been realized experimentally in epilayers. The further understanding of polar behavior of theses phases will be helpful to obtain high 2DEG in Ga_2O_3 based power electronics, especially ε-$(Al_{1-x}Ga_x)_2O_3/Ga_2O_3$ HEMTs [254].

(b) The δ- and κ-Ga_2O_3 are the least explored phases due to their phase instability. Only structural information is available for δ-Ga_2O_3. Therefore, lots of research opportunities are available in this direction but how to achieve pure phase of δ-Ga_2O_3 could be big challenge.

(c) The electrical breakdown of β-Ga_2O_3 materials was found to depend on the material thickness. A thicker film can sustain high breakdown voltage but requires a better thermal optimization during the device implementation. The entire community is still looking for a better thermal management strategy of Ga_2O_3 which is another challenge. We can possibly explore different technologies such as heteroepitaxy or wafer bonding the Ga_2O_3 films with high thermal conductivity substrates to resolve the thermal issues. Furthermore, thermal conductivities of different phases other than β-phase have not been reported yet.

(d) The stability of different polymorphs of Ga_2O_3 were found to depend on growth substrates and doping. Importantly, different substrates and their off-cut angles have strong impact on the material growth which can also be investigated in future by the possible establishment of the growth kinetics of the films grown on different substrates with different doping condition.

(e) The insertion of buffer layer technology to achieve high crystalline quality of Ga_2O_3 epilayer is rarely investigated. The reduced lattice mismatch using buffer layer may result in better quality films with improved electrical and optical properties. Efforts should be continued to control defect, doping, phase stability and phase transition. For example, exploring n-type and p-type doping in different epitaxial layers with various phase could be quite interesting from fundamental as well as application point of view. Also, for the PLD-related growth of Ga_2O_3 material, the effect of laser energy on growth kinetics of Ga_2O_3 thin films has not been optimized in details. Integration of epitaxial Ga_2O_3 on flexible substrates has great potential for future of smart and flexible devices since the epitaxial growth of Ga_2O_3 on flexible substrates is at the early stage of research. In the end, the etching and surface treatments of Ga_2O_3 polymorphs is also critical to obtain high performance devices.

Data availability statement

The data that support the findings of this study are available upon reasonable request from the authors.

Acknowledgments

Dr R Singh is thankful to DST for partial financial support for this work through the BRICS project. Dr H Sun acknowledges the National Science Foundation of China (Grant No. 51961145110) for partial support to this work. Dr B R Tak is thankful to the Department of Science and Technology (DST) INSPIRE PhD fellowship.

ORCID iDs

B R Tak https://orcid.org/0000-0002-6150-9180
Xiaohang Li https://orcid.org/0000-0002-4434-365X
Haiding Sun https://orcid.org/0000-0001-8664-666X
R Singh https://orcid.org/0000-0002-6890-6904

References

[1] Haochen Z, Chen H, Kang S, Huabin Y, Chong X, Danhao W, Zhongling L and Haiding S 2021 *Rep. Prog. Phys.* **84** 044401
[2] Huang C, Zhang H and Sun H 2020 *Nano Energy* **77** 105149
[3] Amano H *et al* 2020 *J. Phys. D: Appl. Phys.* **53** 503001
[4] Zhang X *et al* 2020 *J. Phys. D: Appl. Phys.* **53** 495105
[5] Marezio M and Remeika J P 1967 *J. Chem. Phys.* **46** 1862–5
[6] Bermudez V M 2006 *Chem. Phys.* **323** 193–203
[7] Playford H Y, Hannon A C, Tucker M G, Dawson D M, Ashbrook S E, Kastiban R J, Sloan J and Walton R I 2014 *J. Phys. Chem.* C **118** 16188–98
[8] Cora I, Mezzadri F, Boschi F, Bosi M, Čaplovičová M, Calestani G, Dódony I, Pécz B and Fornari R 2017 *Cryst. Eng. Comm.* **19** 1509–16
[9] Playford H Y, Hannon A C, Barney E R and Walton R I 2013 *Chem. Eur. J.* **19** 2803–13
[10] Yoshioka S, Hayashi H, Kuwabara A, Oba F, Matsunaga K and Tanaka I 2007 *J. Phys.: Condens. Matter* **19** 346211
[11] Mezzadri F, Calestani G, Boschi F, Delmonte D, Bosi M and Fornari R 2016 *Inorg. Chem.* **55** 12079–84
[12] Li Z, Zhao B, Liu P and Zhang Y 2008 *Microelectron. Eng.* **85** 1613–5
[13] Higashiwaki M, Sasaki K, Murakami H, Kumagai Y, Koukitu A, Kuramata A, Masui T and Yamakoshi S 2016 *Semicond. Sci. Technol.* **31** 034001
[14] Higashiwaki M, Sasaki K, Kuramata A, Masui T and Yamakoshi S 2012 *Appl. Phys. Lett.* **100** 013504
[15] Kim J, Oh S, Mastro M A and Kim J 2016 *Phys. Chem. Chem. Phys.* **18** 15760–4
[16] Wong M H, Nakata Y, Kuramata A, Yamakoshi S and Higashiwaki M 2017 *Appl. Phys. Express* **10** 041101
[17] Wong M H, Sasaki K, Kuramata A, Yamakoshi S and Higashiwaki M 2016 *IEEE Electron. Device Lett.* **37** 212–5
[18] Higashiwaki M, Sasaki K, Kamimura T, Wong M H, Krishnamurthy D, Kuramata A, Masui T and Yamakoshi S 2013 *Appl. Phys. Lett.* **103** 123511
[19] Dong H *et al* 2019 *IEEE Electron. Device Lett.* **40** 1385–8
[20] Tak B R, Garg M, Kumar A, Gupta V and Singh R 2019 *ECS J. Solid State Sci. Technol.* **8** Q3149–53
[21] Tak B R and Singh R 2021 *ACS Appl. Electron. Mater.* **3** 2145–51
[22] Tak B R, Garg M, Dewan S, Torres-Castanedo C G, Li K-H, Gupta V, Li X and Singh R 2019 *J. Appl. Phys.* **125** 144501
[23] Feng P, Zhang J Y, Li Q H and Wang T H 2006 *Appl. Phys. Lett.* **88** 153107
[24] Li L, Auer E, Liao M, Fang X, Zhai T, Gautam U K, Lugstein A, Koide Y, Bando Y and Golberg D 2011 *Nanoscale* **3** 1120–6
[25] Hsieh C-H, Chou L-J, Lin G-R, Bando Y and Golberg D 2008 *Nano Lett.* **8** 3081–5
[26] Kumar S, Dhara S, Agarwal R and Singh R 2016 *J. Alloys Compd.* **683** 143–8
[27] Kong W-Y, Wu G-A, Wang K-Y, Zhang T-F, Zou Y-F, Wang D-D and Luo L-B 2016 *Adv. Mater.* **28** 10725–31
[28] Du J, Xing J, Ge C, Liu H, Liu P, Hao H, Dong J, Zheng Z and Gao H 2016 *J. Phys. D: Appl. Phys.* **49** 425105
[29] Cui W, Guo D, Zhao X, Wu Z, Li P, Li L, Cui C and Tang W 2016 *RSC Adv.* **6** 100683–9
[30] López I, Castaldini A, Cavallini A, Nogales E, Méndez B and Piqueras J 2014 *J. Phys. D: Appl. Phys.* **47** 415101
[31] Li Y, Tokizono T, Liao M, Zhong M, Koide Y, Yamada I and Delaunay J-J 2010 *Adv. Funct. Mater.* **20** 3972–8
[32] Higashiwaki M, Sasaki K, Kuramata A, Masui T and Yamakoshi S 2014 *Phys. Status Solidi* a **211** 21–26
[33] Kasu M, Hanada K, Moribayashi T, Hashiguchi A, Oshima T, Oishi T, Koshi K, Sasaki K, Kuramata A and Ueda O 2016 *Japan. J. Appl. Phys.* **55** 1202BB
[34] Sasaki K, Higashiwaki M, Kuramata A, Masui T and Yamakoshi S 2013 *J. Cryst. Growth* **378** 591–5
[35] Higashiwaki M *et al* 2016 *Appl. Phys. Lett.* **108** 133503
[36] Sheoran H, Tak B R, Manikanthababu N and Singh R 2020 *ECS J. Solid State Sci. Technol.* **9** 055004
[37] Tan P *et al* 2021 *Adv. Opt. Mater.* **n/a** 2100173
[38] Hou X *et al* 2020 *J. Appl. Phys.* **54** 043001

[39] Manikanthababu N, Tak B R, Prajna K, Singh R and Panigrahi B K 2020 *Semicond. Sci. Technol.* **35** 055024
[40] Goldschmidt V M, Barth T, Lunde G and Videnskaps-Akad Oslo S N 1925 *I. Mat. Naturv. Klasse* **7** 24
[41] Roy R, Hill V G and Osborn E F 1952 *J. Am. Chem. Soc.* **74** 719–22
[42] Battiston G A, Gerbasi R, Porchia M, Bertoncello R and Caccavale F 1996 *Thin Solid Films* **279** 115–8
[43] Víllora E G, Shimamura K, Yoshikawa Y, Aoki K and Ichinose N 2004 *J. Cryst. Growth* **270** 420–6
[44] Chang P-C, Fan Z, Tseng W-Y, Rajagopal A and Lu J G 2005 *Appl. Phys. Lett.* **87** 222102
[45] Aida H, Nishiguchi K, Takeda H, Aota N, Sunakawa K and Yaguchi Y 2008 *Japan. J. Appl. Phys.* **47** 8506–9
[46] Shinohara D and Fujita S 2008 *Japan. J. Appl. Phys.* **47** 7311–3
[47] Kuramata A, Koshi K, Watanabe S, Yamaoka Y, Masui T and Yamakoshi S 2016 *Japan. J. Appl. Phys.* **55** 1202A2
[48] Higashiwaki M, Kuramata A, Murakami H and Kumagai Y 2017 *J. Phys. D: Appl. Phys.* **50** 333002
[49] Yang J, Ren F, Tadjer M, Pearton S J and Kuramata A 2018 *ECS J. Solid State Sci. Technol.* **7** Q92–Q96
[50] Hu Z *et al* 2018 *IEEE Electron. Device Lett.* **39** 1564–7
[51] Nishinaka H, Ueda O, Tahara D, Ito Y, Ikenaga N, Hasuike N and Yoshimoto M 2020 *ACS Omega* **5** 29585–92
[52] Mastro M A, Kuramata A, Calkins J, Kim J, Ren F and Pearton S J 2017 *ECS J. Solid State Sci. Technol.* **6** P356–9
[53] Tak B R, Yang M-M, Lai Y-H, Chu Y-H, Alexe M and Singh R 2020 *Sci. Rep.* **10** 16098
[54] Tak B R, Dewan S, Goyal A, Pathak R, Gupta V, Kapoor A K, Nagarajan S and Singh R 2019 *Appl. Surf. Sci.* **465** 973–8
[55] Mazzolini P, Falkenstein A, Wouters C, Schewski R, Markurt T, Galazka Z, Martin M, Albrecht M and Bierwagen O 2020 *APL Mater.* **8** 011107
[56] Tadjer M J *et al* 2020 *J. Appl. Phys.* **54** 034005
[57] Mizutani F, Higashi S, Inoue M and Nabatame T 2020 *J. Vac. Sci. Technol.* A **38** 022412
[58] Uno K, Ohta M and Tanaka I 2020 *Appl. Phys. Lett.* **117** 052106
[59] Liu Z, Huang Y, Li H, Zhang C, Jiang W, Guo D, Wu Z, Li P and Tang W 2020 *Vacuum* **177** 109425
[60] Kumar S and Singh R 2013 *Phys. Status Solidi* **7** 781–92
[61] Kumar S, Tessarek C, Christiansen S and Singh R 2014 *J. Alloys Compd.* **587** 812–8
[62] Kumar S, Sarau G, Tessarek C, Bashouti M Y, Hähnel A, Christiansen S and Singh R 2014 *J. Phys. D: Appl. Phys.* **47** 435101
[63] Galazka Z, Uecker R, Irmscher K, Albrecht M, Klimm D, Pietsch M, Brützam M, Bertram R, Ganschow S and Fornari R 2010 *Cryst. Res. Technol.* **45** 1229–36
[64] Irmscher K, Galazka Z, Pietsch M, Uecker R and Fornari R 2011 *J. Appl. Phys.* **110** 063720
[65] Galazka Z, Uecker R, Klimm D, Irmscher K, Naumann M, Pietsch M, Kwasniewski A, Bertram R, Ganschow S and Bickermann M 2016 *ECS J. Solid State Sci. Technol.* **6** Q3007–11
[66] Oishi T, Koga Y, Harada K and Kasu M 2015 *Appl. Phys. Express* **8** 031101
[67] Tomm Y, Ko J M, Yoshikawa A and Fukuda T 2001 *Sol. Energy Mater. Sol. Cells* **66** 369–74
[68] Hu J Q, Li Q, Meng X M, Lee C S and Lee S T 2002 *J. Phys. Chem.* B **106** 9536–9
[69] Choi Y C, Kim W S, Park Y S, Lee S M, Bae D J, Lee Y H, Park G-S, Choi W B, Lee N S and Kim J M 2000 *Adv. Mater.* **12** 746–50
[70] Park G-S, Choi W-B, Kim J-M, Choi Y C, Lee Y H and Lim C-B 2000 *J. Cryst. Growth* **220** 494–500
[71] Kumar M, Kumar V and Singh R 2017 *Nanoscale Res. Lett.* **12** 184
[72] Kumar S, Tessarek C, Sarau G, Christiansen S and Singh R 2015 *Adv. Eng. Mater.* **17** 709–15
[73] Domènech-Gil G, Peiró I, López-Aymerich E, Moreno M, Pellegrino P, Gràcia I, Cané C, Barth S and Romano-Rodríguez A 2018 *Proceedings* **2** 958
[74] Li J-S, Zhang X-D, Cao X, Xu K, Zhang L, Fan Y-M and Zhang B-S 2019 *Nanotechnology* **31** 02LT1
[75] Zhu F, Yang Z, Zhou W and Zhang Y 2006 *Appl. Surf. Sci.* **252** 7930–3
[76] Guo D, Guo Q, Chen Z, Wu Z, Li P and Tang W 2019 *Mater. Today Phys.* **11** 100157
[77] Remeika J P and Marezio M 1966 *Appl. Phys. Lett.* **8** 87–88
[78] Lee S-D, Akaiwa K and Fujita S 2013 *Phys. Status Solidi* c **10** 1592–5
[79] Yan-Mei M, Hai-Yong C, Kai-Feng Y, Min L, Qi-Liang C, Jing L and Guang-Tian Z 2008 *Chin. Phys. Lett.* **25** 1603–5
[80] Riena J, Kentaro K and Shizuo F 2021 *Japan. J. Appl. Phys.* **60** SBBD13
[81] Liu Q, Guo D, Chen K, Su Y, Wang S, Li P and Tang W 2018 *J. Alloys Compd.* **731** 1225–9
[82] Oshima T, Nakazono T, Mukai A and Ohtomo A 2012 *J. Cryst. Growth* **359** 60–63
[83] Geller S 1960 *J. Chem. Phys.* **33** 676–84
[84] Åhman J, Svensson G and Albertsson J 1996 *Acta Crystallogr.* **C52** 1336
[85] Ahmadi E and Oshima Y 2019 *J. Appl. Phys.* **126** 160901
[86] Ueda N, Hosono H, Waseda R and Kawazoe H 1997 *Appl. Phys. Lett.* **71** 933–5
[87] Schubert M *et al* 2016 *Phys. Rev.* B **93** 125209
[88] Kumar A, Singh S, Tak B R, Patel A, Asokan K and Kanjilal D 2021 *Appl. Phys. Lett.* **118** 062102
[89] Ricci F, Boschi F, Baraldi A, Filippetti A, Higashiwaki M, Kuramata A, Fiorentini V and Fornari R 2016 *J. Phys.: Condens. Matter* **28** 224005
[90] He H, Orlando R, Blanco M A, Pandey R, Amzallag E, Baraille I and Rérat M 2006 *Phys. Rev.* B **74** 195123
[91] Oshima T, Matsuyama K, Yoshimatsu K and Ohtomo A 2015 *J. Cryst. Growth* **421** 23–26
[92] Hayashi H, Huang R, Oba F, Hirayama T and Tanaka I 2011 *J. Mater. Res.* **26** 578–83
[93] Nishinaka H, Miyauchi N, Tahara D, Morimoto S and Yoshimoto M 2018 *Cryst. Eng. Comm.* **20** 1882–8
[94] Tahara D, Nishinaka H, Morimoto S and Yoshimoto M 2018 *Appl. Phys. Lett.* **112** 152102
[95] Yusa S, Oka D and Fukumura T 2020 *CrystEngComm* **22** 381–5
[96] Oshima Y, Víllora E G, Matsushita Y, Yamamoto S and Shimamura K 2015 *J. Appl. Phys.* **118** 085301
[97] Kim J, Tahara D, Miura Y and Kim B G 2018 *Appl. Phys. Express* **11** 061101
[98] Zhang Z-C, Wu Y and Ahmed S 2019 *Mater. Res. Express* **6** 125904
[99] Mulazzi M, Reichmann F, Becker A, Klesse W M, Alippi P, Fiorentini V, Parisini A, Bosi M and Fornari R 2019 *APL Mater.* **7** 022522
[100] Zhang T, Li Y, Zhang Y, Feng Q, Ning J, Zhang C, Zhang J and Hao Y 2020 *ECS J. Solid State Sci. Technol.* **9** 065009
[101] Egyenes-Pörsök F, Gucmann F, Hušeková K, Dobročka E, Sobota M, Mikolášek M, Fröhlich K and Ťapajna M 2020 *Semicond. Sci. Technol.* **35** 115002
[102] Cheng Y *et al* 2020 *J. Alloys Compd.* **831** 154776
[103] Muazzam U U, Chavan P, Raghavan S, Muralidharan R and Nath D N 2020 *IEEE Photonics Technol. Lett.* **32** 422–5
[104] Ha M-T, Kim K-H, Kwon Y-J, Kim C-J, Jeong S-M and Bae S-Y 2019 *ECS J. Solid State Sci. Technol.* **8** Q3206–12
[105] Son H, Choi Y-J, Ha J-S, Jung S H and Jeon D-W 2019 *Cryst. Growth Des.* **19** 5105–10

[106] Polyakov A Y *et al* 2020 *ECS J. Solid State Sci. Technol.* **9** 045003
[107] Oshima Y, Kawara K, Oshima T, Okigawa M and Shinohe T 2020 *Japan. J. Appl. Phys.* **59** 025512
[108] Wheeler V D *et al* 2020 *Chem. Mater.* **32** 1140–52
[109] Xu C X, Liu H, Pan X H and Ye Z Z 2020 *Opt. Mater.* **108** 110145
[110] Leach J H, Udwary K, Rumsey J, Dodson G, Splawn H and Evans K R 2019 *APL Mater.* **7** 022504
[111] Sun H, Li K-H, Castanedo C G T, Okur S, Tompa G S, Salagaj T, Lopatin S, Genovese A and Li X 2018 *Cryst. Growth Des.* **18** 2370–6
[112] Wang Q, Chen J, Huang P, Li M, Lu Y, Homewood K P, Chang G, Chen H and He Y 2019 *Appl. Surf. Sci.* **489** 101–9
[113] Ghosh S, Srivastava H, Rao P N, Nand M, Tiwari P, Srivastava A K, Jha S N, Rai S K, Singh S D and Ganguli T 2020 *Semicond. Sci. Technol.* **35** 085024
[114] Kalarickal N K, Xia Z, McGlone J, Krishnamoorthy S, Moore W, Brenner M, Arehart A R, Ringel S A and Rajan S 2019 *Appl. Phys. Lett.* **115** 152106
[115] Wang D, He L, Ma X, Xiao H, Le Y and Ma J 2020 *Mater. Charact.* **165** 110391
[116] Lingaparthi R, Thieu Q T, Koshi K, Wakimoto D, Sasaki K and Kuramata A 2020 *Appl. Phys. Lett.* **116** 092101
[117] Yu J, Wang Y, Li H, Huang Y, Tang W and Wu Z 2020 *J. Phys. D: Appl. Phys.* **53** 24LT01
[118] Mazzolini P and Bierwagen O 2020 *J. Phys. D: Appl. Phys.* **53** 354003
[119] Zhuo Y, Chen Z, Tu W, Ma X, Pei Y and Wang G 2017 *Appl. Surf. Sci.* **420** 802–7
[120] Huang Y, Liu Z, Wang J, Zhi Y, Guo D, Wang X, Wang X, Chen Z, Li P and Tang W 2020 *ECS J. Solid State Sci. Technol.* **9** 055010
[121] Huang Y, Gao A, Guo D, Lu X, Zhang X, Huang Y, Yu J, Li S, Li P and Tang W 2020 *J. Mater. Chem.* C **8** 536–42
[122] Vasanthi V, Kottaisamy M and Ramakrishnan V 2019 *Ceram. Int.* **45** 2079–87
[123] Oka D, Yusa S, Kimura K, Ang A K R, Happo N, Hayashi K and Fukumura T 2019 *Japan. J. Appl. Phys.* **59** 010601
[124] Liu Z, Huang Y, Zhang C, Wang J, Li H, Wu Z, Li P and Tang W 2020 *J. Phys. D: Appl. Phys.* **53** 295109
[125] Nikolaev V I, Stepanov S I, Pechnikov A I, Shapenkov S V, Scheglov M P, Chikiryaka A V and Vyvenko O F 2020 *ECS J. Solid State Sci. Technol.* **9** 045014
[126] Nikolaev V I, Pechnikov A I, Nikolaev V V, Scheglov M P, Chikiryaka A V, Stepanov S I, Medvedev O S, Shapenkov S V, Ubyivovk E V and Vyvenko O F 2019 *J. Phys.: Conf. Ser.* **1400** 055049
[127] Nishinaka H, Komai H, Tahara D, Arata Y and Yoshimoto M 2018 *Japan. J. Appl. Phys.* **57** 115601
[128] Tahara D, Nishinaka H, Noda M and Yoshimoto M 2018 *Mater. Lett.* **232** 47–50
[129] Kuang Y *et al* 2021 *ACS Appl. Electron. Mater.* **3** 795–803
[130] Schultz T, Kneiß M, Storm P, Splith D, von Wenckstern H, Grundmann M and Koch N 2020 *ACS Appl. Mater. Interfaces* **12** 8879–85
[131] Kneiß M, Storm P, Hassa A, Splith D, Wenckstern H V, Lorenz M and Grundmann M 2020 *APL Mater.* **8** 051112
[132] Oshima Y, Kawara K, Oshima T and Shinohe T 2020 *Japan. J. Appl. Phys.* **59** 115501
[133] Shimazoe K, Nishinaka H, Arata Y, Tahara D and Yoshimoto M 2020 *AIP Adv.* **10** 055310
[134] Lee J, Kim H, Gautam L, He K, Hu X, Dravid V P and Razeghi M 2021 *Photonics* **8** 17
[135] Kneiß M, Hassa A, Splith D, Sturm C, Wenckstern H V, Schultz T, Koch N, Lorenz M and Grundmann M 2019 *APL Mater.* **7** 022516
[136] Hassa A, Sturm C, Kneiß M, Splith D, Wenckstern H V, Schultz T, Koch N, Lorenz M and Grundmann M 2020 *APL Mater.* **8** 021103
[137] Yu F-P, Ou S-L and Wuu D-S 2015 *Opt. Mater. Express* **5** 1240–9
[138] Leedy K D *et al* 2018 *APL Mater.* **6** 101102
[139] Tak B R, Gupta V, Kapoor A K, Chu Y-H and Singh R 2019 *ACS Appl. Electron. Mater.* **1** 2463–70
[140] Ou S-L, Wuu D-S, Fu Y-C, Liu S-P, Horng R-H, Liu L and Feng Z-C 2012 *Mater. Chem. Phys.* **133** 700–5
[141] Müller S, von Wenckstern H, Splith D, Schmidt F and Grundmann M 2014 *Phys. Status Solidi* a **211** 34–39
[142] Orita M, Hiramatsu H, Ohta H, Hirano M and Hosono H 2002 *Thin Solid Films* **411** 134–9
[143] Goyal A, Yadav B S, Thakur O P, Kapoor A K and Muralidharan R 2014 *J. Alloys Compd.* **583** 214–9
[144] Zhang F, Arita M, Wang X, Chen Z, Saito K, Tanaka T, Nishio M, Motooka T and Guo Q 2016 *Appl. Phys. Lett.* **109** 102105
[145] Zhang F, Saito K, Tanaka T, Nishio M and Guo Q 2015 *J. Mater. Sci., Mater. Electron.* **26** 9624–9
[146] Zhang F, Saito K, Tanaka T, Nishio M and Guo Q X 2014 *Solid State Commun.* **186** 28–31
[147] Hu Z, Feng Q, Zhang J, Li F, Li X, Feng Z, Zhang C and Hao Y 2018 *Superlattices Microstruct.* **114** 82–88
[148] Kneiß M, Hassa A, Splith D, Sturm C, Wenckstern H V, Lorenz M and Grundmann M 2019 *APL Mater.* **7** 101102
[149] Wakabayashi R, Oshima T, Hattori M, Sasaki K, Masui T, Kuramata A, Yamakoshi S, Yoshimatsu K and Ohtomo A 2015 *J. Cryst. Growth* **424** 77–79
[150] Wellenius P, Smith E R, LeBoeuf S M, Everitt H O and Muth J F 2010 *J. Appl. Phys.* **107** 103111
[151] Chen Z, Saito K, Tanaka T, Nishio M, Arita M and Guo Q 2015 *J. Cryst. Growth* **430** 28–33
[152] Hu G C, Shan C X, Zhang N, Jiang M M, Wang S P and Shen D Z 2015 *Opt. Express* **23** 13554–61
[153] Wei T, Tsai D, Ravadgar P, Ke J, Tsai M, Lien D, Huang C, Horng R and He J 2014 *IEEE J. Sel. Top. Quantum Electron.* **20** 112–7
[154] Ravadgar P, Horng R H, Yao S D, Lee H Y, Wu B R, Ou S L and Tu L W 2013 *Opt. Express* **21** 24599–610
[155] Liu Y D, Liang H W, Xia X C, Shen R S, Liu Y, Bian J M and Du G T 2012 *Appl. Phys.* B **109** 605–9
[156] Liu Y D, Xia X C, Liang H W, Zhang H Z, Bian J M, Liu Y, Shen R S, Luo Y M and Du G T 2012 *J. Mater. Sci., Mater. Electron.* **23** 542–5
[157] Zhang F, Arita M, Wang X, Chen Z W, Saito K, Tanaka T, Nishio M, Motooka T and Guo Q X 2016 *Appl. Phys. Lett.* **109** 100–4
[158] Wang Y Z, Li N, Duan P P, Zhang L L, Chu B L, He Q Y and Qiu J R 2017 *Sci. Adv. Mater.* **9** 403–7
[159] Oshima T, Okuno T and Fujita S 2007 *Japan. J. Appl. Phys.* **46** 7217–20
[160] Guo D Y *et al* 2014 *Opt. Mater. Express* **4** 1067–76
[161] Liu X Z, Guo P, Sheng T, Qian L X, Zhang W L and Li Y R 2016 *Opt. Mater.* **51** 203–7
[162] Kaun S W, Wu F and Speck J S 2015 *J. Vac. Sci. Technol.* A **33** 041508
[163] Krishnamoorthy S *et al* 2017 *Appl. Phys. Lett.* **111** 023502
[164] Vogt P and Bierwagen O 2016 *Appl. Phys. Lett.* **108** 072101
[165] Wong M H, Sasaki K, Kuramata A, Yamakoshi S and Higashiwaki M 2016 *Japan. J. Appl. Phys.* **55** 1202B9
[166] Ahmadi E, Koksaldi O S, Zheng X, Mates T, Oshima Y, Mishra U K and Speck J S 2017 *Appl. Phys. Express* **10** 071101
[167] Asel T J, Steinbrunner E, Hendricks J, Neal A T and Mou S 2020 *J. Vac. Sci. Technol.* A **38** 043403
[168] Kracht M *et al* 2017 *Phys. Rev. Appl.* **8** 054002

[169] Cheng Z, Hanke M, Vogt P, Bierwagen O and Trampert A 2017 *Appl. Phys. Lett.* **111** 162104
[170] Yu Z, Overgaard C D, Droopad R, Passlack M and Abrokwah J K 2003 *Appl. Phys. Lett.* **82** 2978–80
[171] Guo D Y *et al* 2015 *J. Mater. Chem.* C **3** 1830–4
[172] Hao S J *et al* 2019 *J. Appl. Phys.* **125** 105701
[173] Cheng Z, Hanke M, Galazka Z and Trampert A 2018 *Nanotechnology* **29** 395705
[174] Ahmadi E, Koksaldi O S, Kaun S W, Oshima Y, Short D B, Mishra U K and Speck J S 2017 *Appl. Phys. Express* **10** 041102
[175] Oshima T and Fujita S 2008 *Phys. Status Solidi* c **5** 3113–5
[176] Mauze A, Zhang Y, Mates T, Wu F and Speck J S 2019 *Appl. Phys. Lett.* **115** 052102
[177] Zhao X, Wu Z, Zhi Y, An Y, Cui W, Li L and Tang W 2017 *J. Phys. D: Appl. Phys.* **50** 085102
[178] Guo D, Li P, Wu Z, Cui W, Zhao X, Lei M, Li L and Tang W 2016 *Sci. Rep.* **6** 24190
[179] Alema F, Hertog B, Osinsky A, Mukhopadhyay P, Toporkov M and Schoenfeld W V 2017 *J. Cryst. Growth* **475** 77–82
[180] Mi W, Ma J, Luan C, Lv Y, Xiao H and Li Z 2012 *Mater. Lett.* **87** 109–12
[181] Li Z *et al* 2020 *Vacuum* **178** 109440
[182] Cao Q, He L, Xiao H, Feng X, Lv Y and Ma J 2018 *Mater. Sci. Semicond. Process.* **77** 58–63
[183] Mi W, Luan C, Li Z, Zhao C, Xiao H and Ma J 2013 *Mater. Lett.* **107** 83–85
[184] Cao Q, He L, Feng X, Xiao H and Ma J 2018 *Ceram. Int.* **44** 830–5
[185] Wang D, He L, Le Y, Feng X, Luan C, Xiao H and Ma J 2020 *Ceram. Int.* **46** 4568–72
[186] Mi W, Ma J, Zhu Z, Luan C, Lv Y and Xiao H 2012 *J. Cryst. Growth* **354** 93–97
[187] Boschi F, Bosi M, Berzina T, Buffagni E, Ferrari C and Fornari R 2016 *J. Cryst. Growth* **443** 25–30
[188] Chen Y, Xia X, Liang H, Abbas Q, Liu Y and Du G 2018 *Cryst. Growth Des.* **18** 1147–54
[189] Hou X, Sun H, Long S, Tompa G S, Salagaj T, Qin Y, Zhang Z, Tan P, Yu S and Liu M 2019 *IEEE Electron. Device Lett.* **40** 1483–6
[190] Qin Y *et al* 2019 *IEEE Electron. Device Lett.* **40** 1475–8
[191] Qin Y *et al* 2020 *ACS Photonics* **7** 812–20
[192] Kim D H, Yoo S H, Chung T M, An K S, Yoo H S and Kim Y 2002 *B Korean Chem. Soc.* **23** 225–8
[193] Kim H W and Kim N H 2004 *Appl. Surf. Sci.* **230** 301–6
[194] Kim H W and Kim N H 2005 *J. Alloys Compd.* **389** 177–81
[195] Lee H, Kim K, Woo J J, Jun D J, Park Y, Kim Y, Lee H W, Cho Y J and Cho H M 2011 *Chem. Vapor Depos.* **17** 191–7
[196] Lv Y, Ma J, Mi W, Luan C N, Zhu Z and Xiao H D 2012 *Vacuum* **86** 1850–4
[197] Guo P, Xiong J, Zhao X H, Sheng T, Yue C, Tao B W and Liu X Z 2014 *J. Mater. Sci., Mater. Electron.* **25** 3629–32
[198] Mi W, Du X J, Luan C N, Xiao H D and Ma J 2014 *RSC Adv.* **4** 30579–83
[199] Mi W, Ma J, Li Z, Luan C N and Xiao H D 2015 *J. Mater. Sci., Mater. Electron.* **26** 7889–94
[200] Feng X J, Li Z, Mi W, Luo Y and Ma J 2015 *Mater. Sci. Semicond. Process.* **34** 52–57
[201] Feng X J, Li Z, Mi W and Ma J 2016 *Vacuum* **124** 101–7
[202] Kong L Y, Ma J, Luan C N, Mi W and Lv Y 2012 *Thin Solid Films* **520** 4270–4
[203] Du X J, Mi W, Luan C N, Li Z, Xia C T and Ma J 2014 *J. Cryst. Growth* **404** 75–79
[204] Mi W, Li Z, Luan C N, Xiao H D, Zhao C S and Ma J 2015 *Ceram. Int.* **41** 2572–5
[205] Mi W, Luan C N, Li Z, Zhao C S, Feng X J and Ma J 2013 *Opt. Mater.* **35** 2624–8
[206] Mi W, Zhang K L, Zhao J S and Yang Z C 2016 *J. Mater. Sci., Mater. Electron.* **27** 11390–5
[207] Li S, Jiao S, Wang D, Gao S and Wang J 2018 *J. Alloys Compd.* **753** 186–91
[208] Schurig P, Couturier M, Becker M, Polity A and Klar P J 2019 *Phys. Status Solidi* a **216** 1900385
[209] Li M-Q, Yang N, Wang G-G, Zhang H-Y and Han J-C 2019 *Appl. Surf. Sci.* **471** 694–702
[210] Arora K, Goel N, Kumar M and Kumar M 2018 *ACS Photonics* **5** 2391–401
[211] Jianjun L, Jinliang Y, Liang S and Ting L 2010 *J. Semicond.* **31** 103001
[212] Chengyang X 2013 *J. Semicond.* **34** 103004
[213] Zhuang H H, Yan J L, Xu C Y and Meng D L 2014 *Appl. Surf. Sci.* **307** 241–5
[214] Chang S J, Wu Y L, Weng W Y, Lin Y H, Hsieh W K, Sheu J K and Hsu C L 2014 *J. Electrochem. Soc.* **161** H508–11
[215] Kikuchi K, Imura S, Miyakawa K, Ohtake H, Kubota M and Ohta E 2015 *Sens. Actuators* A **224** 24–29
[216] Zhi Y S, Li P G, Wang P C, Guo D Y, An Y H, Wu Z P, Chu X L, Shen J Q, Tang W H and Li C R 2016 *AIP Adv.* **6** 015215
[217] Shigetoshi Y, Tsukimoto S, Takeda H, Ito K and Murakami M 2007 *Mater. Sci. Forum* **561–565** 1233–126
[218] Kumar S S, Rubio E J, Noor-A-Alam M, Martinez G, Manandhar S, Shutthanandan V, Thevuthasan S and Ramana C V 2013 *J. Phys. Chem.* C **117** 4194–200
[219] Akazawa H 2016 *Vacuum* **123** 8–16
[220] Ishibashi K, Aida R, Takahara M, Kudo J, Tsunoda I, Takakura K, Nakashima T, Shibuya M and Murakami K 2013 *Phys. Status Solidi* c **10** 1588–91
[221] Ramana C V, Rubio E J, Barraza C D, Gallardo A M, McPeak S, Kotru S and Grant J T 2014 *J. Appl. Phys.* **115** 043508
[222] Kim K-H, Ha M-T, Kwon Y-J, Lee H, Jeong S-M and Bae S-Y 2019 *ECS J. Solid State Sci. Technol.* **8** Q3165–70
[223] Hao J G *et al* 2020 *Appl. Surf. Sci.* **513** 145871
[224] Jinno R, Uchida T, Kaneko K and Fujita S 2018 *Phys. Status Solidi* b **255** 1700326
[225] Tahara D, Nishinaka H, Morimoto S and Yoshimoto M 2017 *Japan. J. Appl. Phys.* **56** 078004
[226] Lee S-D, Ito Y, Kaneko K and Fujita S 2015 *Japan. J. Appl. Phys.* **54** 030301
[227] Nishinaka H, Tahara D, Morimoto S and Yoshimoto M 2017 *Mater. Lett.* **205** 28–31
[228] Ito H, Kaneko K and Fujita S 2012 *Japan. J. Appl. Phys.* **51** 100207
[229] Akaiwa K, Ota K, Sekiyama T, Abe T, Shinohe T and Ichino K 2020 *Phys. Status Solidi* a **217** 1900632
[230] Chikoidze E, Bardeleben H J V, Akaiwa K, Shigematsu E, Kaneko K, Fujita S and Dumont Y 2016 *J. Appl. Phys.* **120** 025109
[231] Akaiwa K and Fujita S 2012 *Japan. J. Appl. Phys.* **51** 070203
[232] Sheng J, Park E J, Shong B and Park J-S 2017 *ACS Appl. Mater. Interfaces* **9** 23934–40
[233] O'Donoghue R, Rechmann J, Aghaee M, Rogalla D, Becker H-W, Creatore M, Wieck A D and Devi A 2017 *Dalton Trans.* **46** 16551–61
[234] Shi F, Han J, Xing Y, Li J, Zhang L, He T, Li T, Deng X, Zhang X and Zhang B 2019 *Mater. Lett.* **237** 105–8
[235] Wang H, Chen H, Li L, Wang Y, Su L, Bian W, Li B and Fang X 2019 *J. Phys. Chem. Lett.* **10** 6850–6
[236] Tao J, Lu H-L, Gu Y, Ma H-P, Li X, Chen J-X, Liu W-J, Zhang H and Feng J-J 2019 *Appl. Surf. Sci.* **476** 733–40
[237] Mahmoodinezhad A, Janowitz C, Naumann F, Plate P, Gargouri H, Henkel K, Schmeißer D and Flege J I 2020 *J. Vac. Sci. Technol.* A **38** 022404

[238] Altuntas H, Donmez I, Ozgit-Akgun C and Biyikli N 2014 *J. Alloys Compd.* **593** 190–5
[239] Roberts J W, Chalker P R, Ding B, Oliver R A, Gibbon J T, Jones L A H, Dhanak V R, Phillips L J, Major J D and Massabuau F C P 2019 *J. Cryst. Growth* **528** 125254
[240] Larsson F, Keller J, Primetzhofer D, Riekehr L, Edoff M and Törndahl T 2019 *J. Vac. Sci. Technol.* A **37** 030906
[241] Comstock D J and Elam J W 2012 *Chem. Mater.* **24** 4011–8
[242] Shan F K, Liu G X, Lee W J, Lee G H, Kim I S and Shin B C 2005 *J. Appl. Phys.* **98** 023504
[243] Ramachandran R K, Dendooven J, Botterman J, Pulinthanathu Sree S, Poelman D, Martens J A, Poelman H and Detavernier C 2014 *J. Mater. Chem.* A **2** 19232–8
[244] Liu G X, Shan F K, Lee W J, Shin B C, Kim S C, Kim H S and Cho C R 2007 *Integr. Ferroelectr.* **94** 11–20
[245] Liu G X, Shan F K, Park J J, Lee W J, Lee G H, Kim I S, Shin B C and Yoon S G 2006 *J. Electroceram.* **17** 145–9
[246] Liu G X, Shan F K, Lee W J, Lee G H, Kim I S and Shin B C 2006 *Integr. Ferroelectr.* **85** 155–64
[247] Allen T G, Ernst M, Samundsett C and Cuevas A 2015 *IEEE J. Photovolt.* **5** 1586–90
[248] Allen T G and Cuevas A 2015 *Phys. Status Solidi* **9** 220–4
[249] Allen T G and Cuevas A 2014 *Appl. Phys. Lett.* **105** 031601
[250] Alaie Z, Nejad S M and Yousefi M H 2015 *Mater. Sci. Semicond. Process.* **29** 16–55
[251] Altuntas H, Donmez I, Ozgit-Akgun C and Biyikli N 2014 *J. Vac. Sci. Technol.* A **32** 041504
[252] Dezelah C L, Niinisto J, Arstila K, Niinisto L and Winter C H 2006 *Chem. Mater.* **18** 471–5
[253] Donmez I, Ozgit-Akgun C and Biyikli N 2013 *J. Vac. Sci. Technol.* A **31** 01A110
[254] Song K, Zhang H, Fu H, Yang C, Singh R, Zhao Y, Sun H and Long S 2020 *J. Phys. D: Appl. Phys.* **53** 345107